Investigation of Ligand Exchange on CdSe Quantum Dots via DART-MS

By

Amadou M. Fall

A Thesis Submitted in Partial Fulfillment of the Requirements for the Degree of Master of Science in Chemistry

Middle Tennessee State University

December, 2024

Thesis Committee:

Dr. P. Gregory Van Patten, Chair

Dr. Mengliang Zhang

Dr. Keying Ding

ACKNOWLEDGMENTS

I would like to thank my supervisor and mentor Dr. Van Patten for his patience, guidance, and time over the course of this multi-year project.

I would like to thank my committee members, Dr. Zhang for all his help with everything related to DART-MS and Dr. Ding for her help and support.

I would also like to thank my friends from here at MTSU to places all over the world, various undergraduates and graduate students that I have worked with over these years, the Chemistry Department at MTSU and all the faculty and staff who make it what it is and the loads of help and support that have been given to me.

Most importantly, I would like to acknowledge my family. From one sister who helped me push through the thesis writing process to another that has been an anchor and constant support in many of the trials and tribulations in all phases of my life during this project. My parents, my siblings, my late grandmother, for the absolutely ridiculous amount of love and support over the past seven plus years that I will never be able to adequately explain even if this section was as long as the rest of this document. I will forever be grateful for everything they have done for me from long before I began my Master's until now. I love you all.

This work was supported by Grant Award DE-SC0021197 from the Solar Photochemistry program of the Office of Basic Energy Sciences, U.S. Department of Energy.

DEDICATION

For my Grandma and my nephew, Elliott

ABSTRACT

Quantum dots (QDs) are an important part of many aspects of modern chemistry. Ligands play a large part in the ability to functionalize QDs. Specialized ligands, however, are ill-equipped to withstand the high temperatures of colloidal synthesis used to synthesize QDs. Ligand exchange is often used to remove the ligands used in synthesis to place ligands that are more suited to the purpose needed. One issue with ligand exchange is tracking the change of the ligands from the beginning ligand to the new ligand. NMR is sometimes used to track the exchange but it has its drawbacks. In this thesis, a method of Direct Analysis in Real-Time Mass Spectrometry (DART-MS) will be used to track the exchange for the first time. Oleate-capped CdSe QDs are made before being exchanged with dodecylamine (DDA) in increasing amounts. DART-MS is then successfully used to examine the progress of the exchange as oleate is lost from the surface and DDA is increasingly added.

TABLE OF CONTENTS

LIST OF FIGURES

LIST OF EQUATIONS/TABLES

CHAPTER ONE

1.1 What is a Quantum Dot?

Quantum dots (QDs) (Figures 1,2) are nanosized semiconductor particles on the order of 1 to 10 nm, which exhibit differences in their optical, electronic, and physical properties as compared to their bulk phase due to their small size. One of the main hallmarks of these changes is that the material undergoes a phenomenon known as "quantum confinement." Quantum confinement occurs when the particle is reduced to a size smaller than the exciton Bohr radius. The Bohr radius can be generally described as the distance between the nucleus of the hydrogen atom and the electron in the ground state. However, in relationship to the particle the equation can be figured to be as follows

$$a_B = \varepsilon \frac{m}{m^*} a_0$$

Equation 1: Where ε is the dielectric constant of the material, m^* is the reduced mass of an electron-hole pair, m is the rest mass of the electron, and a_0 is the Bohr radius of the hydrogen atom.

When considered in a QD, the Bohr radius can be described as the regular and unobstructed distance between an electron and its hole pair. The relative strength of the confinement within nanoparticles can be determined by calculating the Bohr radii of three separate aspects of the particle, the electron (a_e), the hole (a_h), and the exciton (a_{ex}). When calculating the Bohr radius for the exciton, the value for m^* that is to be used is its reduced mass. When the radius of the nanoparticle is smaller than a_e, a_h, and a_{ex} this is referred to as being strongly confined. When radius of the nanoparticle is less than only one of either a_h, or a_{ex}, it is referred to being intermediately confined. When the radius is greater than both a_h, and a_{ex}, it is referred to being weakly confined. These confinement regimes cause additional amounts of energy to be added to the band gap. As the nanoparticle is a semiconductor, the band gap governs its electronic capabilities due to the unique spacing between the valence band and conduction band. However, as the QD gets smaller, it loses more contributing orbitals that add to the valance and conduction bands. When this occurs, the energy states become discrete instead of continuous as the amount of orbitals decrease. As a result, the band gap of the material increases causing a blue shift in the wavelengths of light released since the valence and conduction bands lose a portion of their density.

Figure 1: CdSe QDs under white light

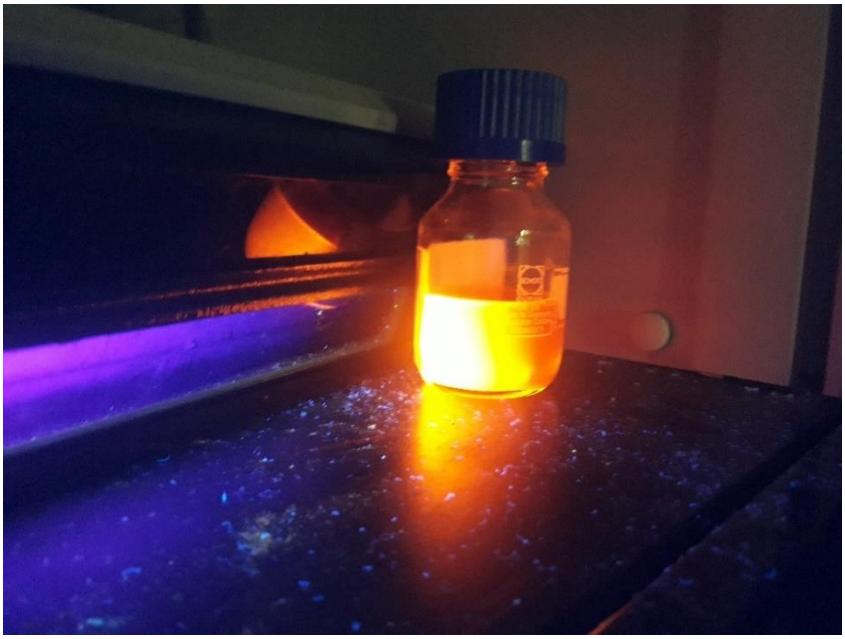

Figure 2: CdSe QDs under ultraviolet light

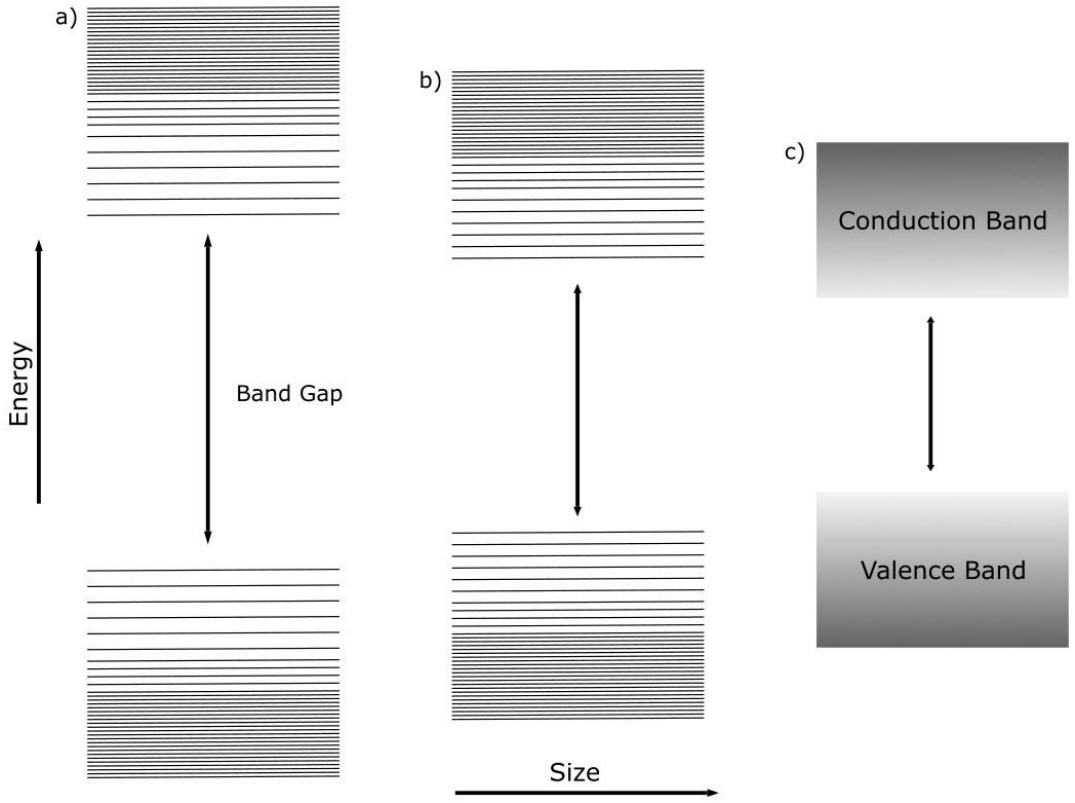

Figure 3: The band gap as seen in (from left to right) a) a small sized quantum dot, b) a large sized quantum dot, and c) the bulk phase of the same material.

To get a more detailed picture of why quantum dots have size-dependent qualities, a speculative approach is needed. A basic approach to comparing quantum dots is a theoretical system known as a particle in a box. This is a hypothetical system where a particle exists in a 1-dimensional box where its walls are potential energy of an infinite value. This causes the particle to be both trapped in the box and forbidden from the boundaries, resulting in the energy of the particle never reaching zero. From a quantum mechanical perspective solving the Schrodinger equation gives the equation $E_n = \frac{n^2 h^2}{8mL^2}$ where E_n is the energy at level n, n is a positive integer, h is Planck's constant, m is the mass of the particle, and L is the length of the box. This gives the allowed energies for the particle.

This causes any electron to only be able to reside at fixed energy levels. The length of the box plays a significant role in determining the highest occupied molecular orbital, lowest unoccupied molecular orbital (HOMO-LUMO) gap in the material. When L is a large value, E_n remains a small value for many values of n . As this happens, orbitals remain near indistinguishable as to create a band. However, when L is a small value, E_n increases between orbitals to a point where there are noticeable gaps between successive orbitals (Figure 3), this causes energy needed to move from successive energy levels increases.

Emission of a photon from a QD occurs when a photon of high enough energy is absorbed to excite an electron from the highest occupied orbital in valence band to the lowest unoccupied orbital in the conduction band. After this electron is excited to a higher energy level, it leaves behind a positively charged hole in its place. When the electron later relaxes and returns to its ground state, it recombines with the hole and releases energy in the form of light. This light's

wavelength corresponds to the energy of the band gap of the material; this is realized when the energy is released as a photon.

One of the effects of this occurrence is that when UV light is shone on the QDs (Figure 2), the wavelength of the emitted photon can change, leading to a veritable rainbow of colors from the same material. These aspects are at their peak in a perfect crystalline structure. However, this is rarely the case as there are often imperfections in the lattice which cause irregularities in the band makeup. One of these irregularities is known as an incomplete combination. This occurs when there is not a completely empty gap between the valence and conduction bands, these areas are sometimes called defects or trap states. When this happens, instead of the electron relaxing from the conduction band back to the valence band, both charge carriers can localize on the defect state causing them to recombine non-radiatively.

In addition to size, the shape of the particle can also have an influence on its properties. QDs can come in a variety of shapes including rods, cones and pyramids.[1] These unique features can be exploited by adjusting the size of the particles to give the desired property. Quantum dots have an enormous surface area in relation to their size and this causes the surface to become extremely important to their functionality.[2]

1.2 How are they made?

One of the more common paths this project uses is colloidal synthesis[3], whereby the QDs are made in solution. A Schlenk line is used for this setup to control the atmosphere for the QDs synthesis as many steps require an inert environment. The synthesis is often done by using a salt of the target metal that is soluble in a mixture of a high boiling point liquid, such as octadecene (ODE), and a suitable coordinating ligand, such as tri-octyl phosphine oxide (TOPO). Afterward, depending on the setup, oxygen is purged from the solution by flowing nitrogen gas through the flask for an hour. Next, the target anion is injected into the flask in a separate suitable solution before leaving to react for a length of time, which can be anywhere from one minute to two hours. After the required time for synthesis, the mixture is then quenched with the addition of a lower boiling point liquid such as butanol to cease the growth of the nanoparticles. The QDs are then separated via centrifuge and stored in a suitable, generally nonpolar solvent such as hexane. Applications of QDs have steadily increased as time has gone by. One of the more prominent aspects that QD researchers have been involved in is alternative energy.[45] The use of QDs in solar cells has reached over 18%[6] as of 2019. Beyond energy, medicine is another highly sought-after field among QD scientists[7]. The fluorescence, as seen in (Figure 2) has led researchers into the uses of nanoparticles in LEDs[8].

1.3 Ligands

A ligand is an atom or molecule that is coordinated with a metal to form a complex. This can be done by sharing or donating an electron to the more central chemical. In the case of QDs, they are mostly organic compounds that either attach to a metal or non-metal atom on the surface. They can come in three different categories. The L-type is made of Lewis bases and attaches to the metal atom. Next are X-type which are single electron donors and can attach to both the metal and non-metal. Lastly comes Z-type which are Lewis acids, itself having a metal atom which then attaches to the non-metal atom of the QD.

In QD usage, ligands also play a vital role in several stages of the QD synthesis process. During synthesis, ligands assist with the controlled growth of QDs, allowing more monodispersed particles.[9–12] Depending on the functional group at the end of a ligand, they can cause a QD to be soluble in polar or nonpolar solvents. During colloidal synthesis of QDs, high boiling point nonpolar solvents, such as octadecane, are used as they have long hydrocarbon chains. This will cause the QDs to be suspended in liquids such as toluene or hexanes.

The bonding and energy levels between ligands and QDs are crucial, as the bonding between the two compounds removes the orbitals that exist in the QD due to crystal imperfections. As a result of this, surface passivation occurs, which allows them to have better opto-electronic properties by reducing trap states and making more efficient quantum dots.[13] This passivation can help ameliorate any issues with surface defects during the synthesis of the QDs due to incomplete coverage of the QDs. Surface defects can cause premature recombination from the charge carrier, decreased quantum yield, and lessened catalytic activity.

1.4 Ligand Exchange

Ligand exchange is a process whereby the organic molecules that were used in the synthesis to coat the QDs are replaced by another set of organic molecules. One of the goals behind this is functionalizing the ligands for the desired purpose such as catalysis, drug delivery, improving their photoluminescent qualities, or changing their solubility. Ligand exchange can be especially useful when attempting to use specialized ligands that cannot withstand the high temperatures needed during synthesis. Additionally, ligand exchange allows the addition of short-chained ligands that would otherwise be impossible to be used as they would lead to the agglomeration of the QDs during the synthesis. With this change of ligand from a long-chain to a short-chain one, a QD can change from being dissolved in a nonpolar solvent such as toluene, into a polar solvent such as water. This allows different types of chemistry to be done, such as catalysis for hydrogen production from water.

The ligand exchange process is governed by the strength of the bond the ligand has to the surface of the material. Quantum dot-ligand interactions consist of a dynamic system where ligands are constantly being attached and detached from the surface of the quantum dot while in a solution. Much like other equilibrium processes, temperature, concentration, and pressure can affect the rate of exchange. When exchanging ligands, the concentration of both the original ligand and of the one being replaced is important. As the concentration of a displacing ligand increases in the system where the exchange is taking place, equilibrium will favor the new ligand being attached to the surface.

1.5 Characterization

1.5.1 UV/Vis/NIR Spectrophotometry

Spectrophotometry is a technique used to measure how well a material absorbs radiation of differing wavelengths by examining which wavelengths remain unaffected when reaching a detector such as a photomultiplier tube. The spectrophotometer has light sources necessary for the required wavelengths. A deuterium lamp is generally used for the UV range, and a tungsten lamp for the visible spectra. This light is then split into two beams that will each target its own cuvette. Before gathering data, one quartz cuvette containing a solvent is used as a reference, and a second cuvette will contain the analyte dissolved in the same solvent as the reference. At this point of measurement, the two beams simultaneously traverse the reference and the sample and are detected so their ratio for transmittance, or the logarithm of their ratio for absorbance can be determined electronically.

Absorbance is a quality unique to a material that describes the amount of light transmitted into a particular medium compared to the amount of light that exits the medium. Light at certain wavelengths can be absorbed by the medium in differing amounts according to the exact energy needed to advance electrons to a higher energy level.

$$A = \varepsilon bc$$

Equation 2: the Beer-Lambert Law describing absorbance, where A= absorbance, ε = molar absorptivity ($Lmol^{-1}cm$), b = molar concentration of the analyte, c = the length of the cuvette (cm)

As one of the more powerful tools used to characterize QDs, spectroscopy is a quick method to characterize the QDs made. With an easily tuned band gap, the amount of light absorbed at a particular wavelength can be used to pinpoint a particular structure (**Figure 3**). In this project, absorbance will be used for a rather fast approach to detecting any change that might have happened during the exchange.

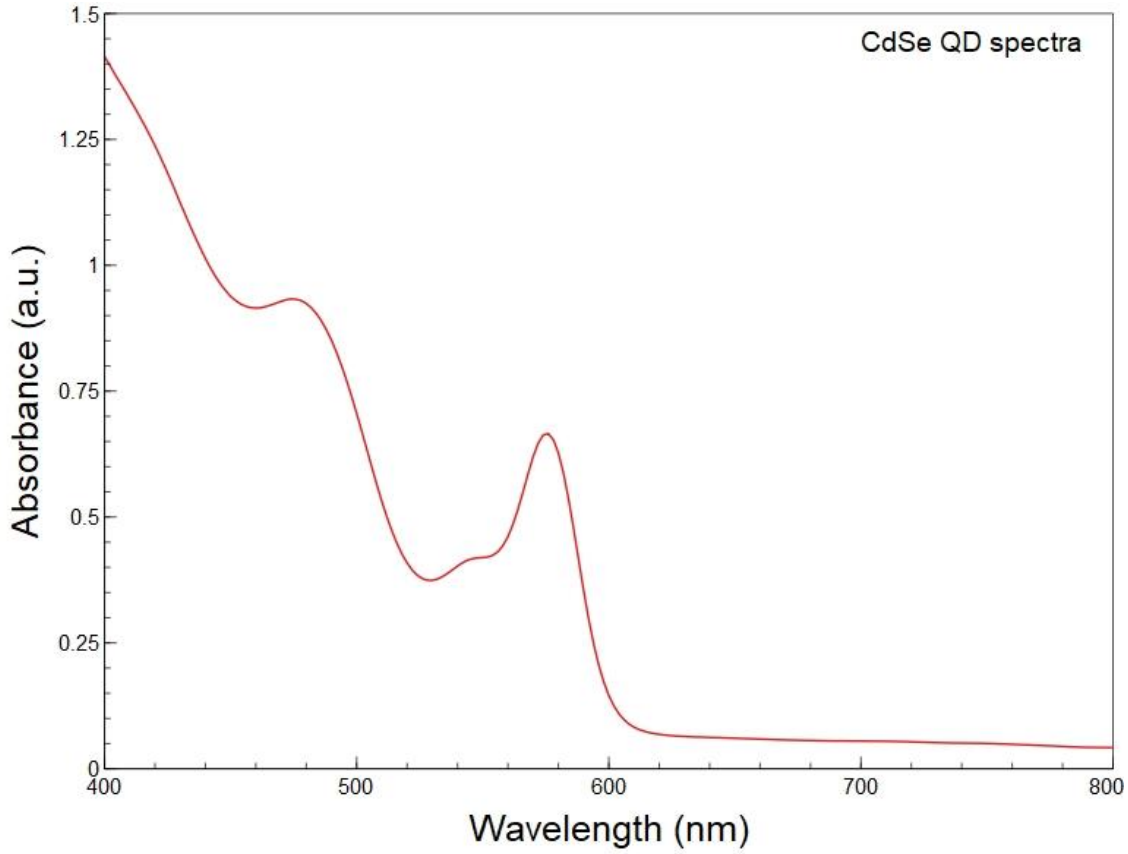

Figure 4: UV-Vis spectrum of CdSe quantum dots

1.5.2 Transmission Electron Microscopy (TEM)

At its core, TEM is essentially an extremely powerful microscope with a resolution thousands of times higher than a conventional microscope. As QDs are often on the nanometer scale, TEM is vital to determine the shape and size of the QDs. This occurs by having an electron beam transmitted through a given sample from a source at the top of the instrument. These electrons then pass through the sample before hitting a screen at the bottom of the microscope where an image is then revealed.

1.5.3 Direct analysis in real-time mass spectrometry (DART-MS)

DART is a relatively new ionization method for ambient mass spectrometry used with an inert gas such as helium.[14,15] A very strong electric potential is applied that helps produce a collection of ions and excited state particles, including the active species being the metastable helium atoms. These species will interact with the available particles in the atmosphere, such as oxygen and water, whose ions will in turn react with organic molecules. The DART-MS can be done in positive and negative modes. Positive mode is when positively charged molecules are generated and monitored (Scheme 1). Throughout this thesis positive mode is mainly used.

$$nH_2O + He^* \rightarrow [(H_2O)_p + H]^+ + [(H_2O)_q + OH]^- + He$$

$$[(H_2O)_p + H]^+ + L \rightarrow pH_2O + [H + L]^+$$

Scheme 1: The reaction that is undergone in the DART ion source in positive mode.[16]

In this experiment, the thermal desorption module was coupled with the DART-MS. He gas flows from a tank before reaching the ion source where it becomes metastable. A copper pot sits on as heating source that can be controlled independently to heat to a specific temperature at a specific rate. It is necessary for the ligands to first desorb from the QDs before reaching a gaseous stage where it will then react with the ionized species. While running the experiment, care must be taken that the rate of temperature increase does not degrade the ligands before reacting. The desorbed molecules flow into a T-tube where it reacts with the excited He ions before entering the mass spectrometer where they are analyzed.

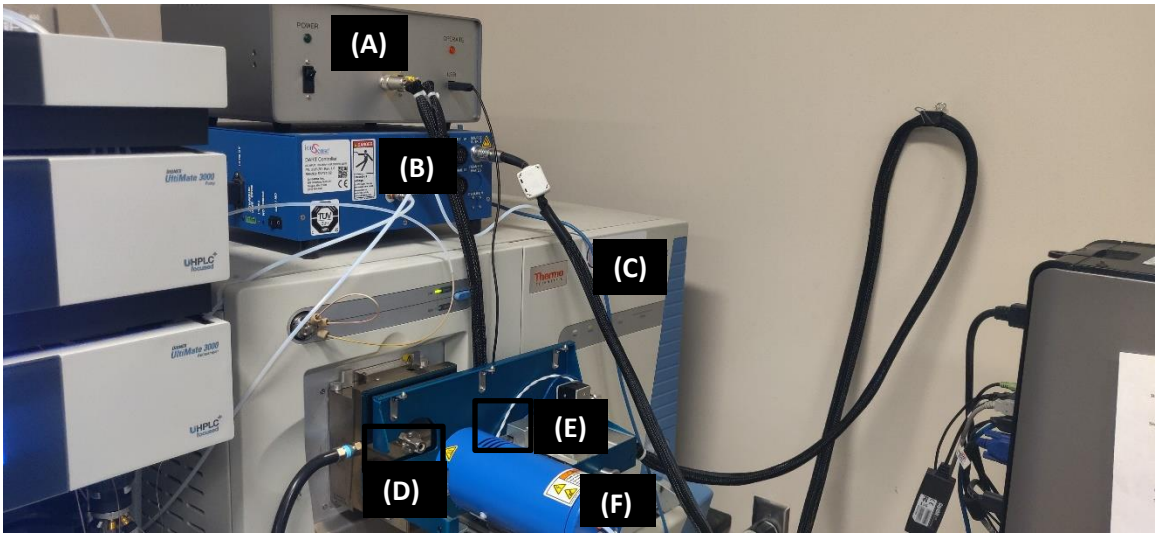

Figure 5: The setup for the DART MS. (A) is the temperature controller for the sample heating element. (B) is the DART controller for the ion source. (C) is the mass spectrometer. (D) is the entrance into the mass spectrometer. (E) is the sample holder/heating element. (F) is the DART ion source.

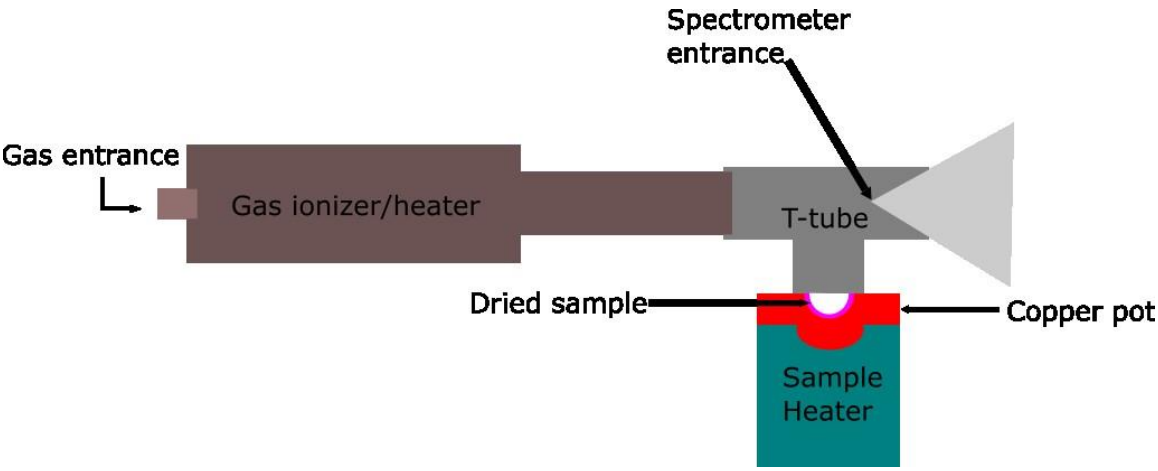

Figure 6: A not-to-scale representation (D), (E), and (F) from Figure 5[16]

1.5.4 Nuclear Magnetic Resonance (NMR)

While not specifically used in this thesis, NMR is a useful tool for determining the complete structure of various organic compounds. It works by generating a very strong magnetic field from a superconducting magnet. Under the influence of the field, the nucleus of different atoms reorient themselves. Radio waves are then applied to the nuclei and will be absorbed at different frequencies (300 to 800 MHz). As the name suggests, the nucleus of the atom resonates because of this electromagnetic frequency and will release different signals which are then detected.

1.6 Goals

The work in this thesis aimed to demonstrate the use of a novel DART-MS method to investigate ligand exchange on the surface of quantum dots. Previous research in our lab has shown that DART-MS can be used to differentiate between bound and unbound ligands on the surface of QDs.[17] Previous cases[18,19] have used NMR to track changes in the ligand composition on the surface of quantum dots, however this method is limited in scope. The main goal of this project was to use DART-MS to examine the gradual loss of the oleate ligand and the gain of dodecylamine on the surface of CdSe quantum dots over the course of ligand exchange. Cadmium oleate was synthesized as the precursor to the cadmium selenide QDs. By using a series of concentrations of dodecylamine solutions, ligand exchange was performed. Characterization was done by UV-VIS spectrometer, DART-MS, and TEM. Analysis of the thermal desorption data was used to track the change of the ligand exchange.

CHAPTER TWO

2.1 Materials

Pre-cleaned 2 mL clear screw cap vials were obtained from Supelco. 1-dodecylamine 98% was obtained from Alfa Aesar. Toluene 99.5%, oleylamine technical grade 70%, oleic acid technical grade 90%, 1-octadecene technical grade 90%, selenium pellets, <5 mm particle size ≥ 99.999% trace metal basis, and acetonitrile 99.5+% A.C.S. reagent were obtained from Sigma-Aldrich. n-hexadecyl palmitate 98% was obtained from Arcos Organics. 365 nm UV Lamp was obtained from Analytik Jena. Carbon film 300 mesh copper TEM grid was obtained from Electron Microscopy Sciences.

2.2 Methods

2.2.1 Synthesis of the cadmium oleate

Using a modified synthesis from Hamachi,[20] cadmium oxide and acetonitrile were placed into a 100 mL round bottom flask. This brown suspension was then stirred for 10 minutes with a magnetic stir bar in an ice bath. At this point, trifluoroacetic acid (fixed amount) and trifluoracetic anhydride (in excess) were added slowly to the mixture. After 15 minutes, the solution became clear and was allowed to reach room temperature.

In a 500 mL Erlenmeyer flask, oleic acid, isopropanol, and triethylamine were mixed together before the cadmium trifluoroacetate solution was then added, forming a white precipitate. This was heated under reflux until the precipitate dissolved and the solution became colorless. The heat was turned off, and the flask was left to cool to room temperature for over two hours, after which it was then further cooled in a freezer at -20 ℃ for another two hours. At this point, a white precipitate reforms and is then purified via suction distillation in a glass fritted funnel and the filtrate is washed 3 times with methanol before being dried under vacuum for 6 hours. The powder is then stored in an oxygen and water-free atmosphere.

2.2.2 Synthesis of the Oleate-capped QDs

CdSe was synthesized using a modified procedure from Fritzinger et al. as these produced high quality QDs that did not use any phosphine ligands during the synthesis.[21] Using 0.2565 g of cadmium oleate, at an equivalent molar amount of the cadmium in cadmium oxide from the original procedure, along with 0.8224 g of oleic acid were weighed on a balance and placed in a 100 mL 3-neck round bottom flask connected to a Schlenk line and condenser cooled by flowing water. 12 mL of ODE was used as a solvent solution and was heated for 1 hour at 100 C on a heating mantle with a needle sticking out of a rubber septum to vent, allowing any moisture to escape with the flowing nitrogen. The solution remained clear throughout the hour it was being heated.

In a separate reaction, using a 50 mL 3-neck round bottom flask connected to a similar setup as the cadmium solution, 0.1264 g of Se was weighed using an analytical balance and 16 mL

of ODE using a plastic syringe. The two reagents were added to the round bottom flask and care was taken as the mixture was heated under nitrogen gas for two hours at 195 °C. Jasieniak reported that when heated at these elevated temperatures for over four hours, it rendered the solution inactive.[22] After completion, the solution was then allowed to cool to room temperature. Over the course of the two hours, the solution went from a gray cloudy solution to a yellow solution to an orange solution and back to yellow as the temperature went down.

As the selenium solution cooled, the cadmium oleate solution was then heated to 265 °C and 3.6 mL of the selenium solution was injected into the hot cadmium mixture. It was left to react at approximately 235 °C for 11 minutes as the color of the solution changed from clear before the injection to yellow at the initial injection, orange after a few seconds to deep red as the reaction progressed. The heating mantle was removed and allowed to cool down to room temperature with no interference. After it was cooled, the solution lightened slightly from the deep red and was placed in two 20 mL glass vials.

2.2.3 Purification

To purify QDs from the initial reaction, 3 mL of the CdSe stock solution was taken out and placed in a 50 mL plastic centrifuge tube. An equivalent volume of toluene was added to it along with a few drops of acetonitrile until the solution became cloudy. It was then centrifuged for 3 min at an RCF of 10378. After the CdSe is precipitated, it is then dissolved in 5 mL of toluene before being split into 10 different 1.5 mL centrifuge tubes and centrifuged for 3 min at an RCF of 17000. The CdSe is then dissolved into 5 mL of toluene a second time, split into 10 different centrifuge

tubes and centrifuged for a further 3 min at an RCF of 17000. The CdSe at this point is dissolved in toluene and accumulated in a single 2 mL glass vial.

2.2.4 Ligand Exchange

As DART-MS is a relatively new method for investigating the surface of QDs, a method of establishing the ability to track changes and the amount of change along the surface is needed.

2.2.4.1 Calculations

Table 1: Table containing the amount of ligand and toluene added to create the solutions of each desired concentration.

Relative Concentration of ligand solution	Added ligand solution (µL)	Compensatory toluene added (µL)
0.0	0.0	417.6
1.0	52.2	365.4
2.0	104.4	313.2
4.0	208.8	208.8
8.0	417.6	0

$$\frac{3\ \times 10^{-3}(L) \times stock\ soln.conc.(M) \times (surf.area\ of\ QD\ (nm^2) \times 4\ {}^{ligands}/_{nm^2} \times 185.23\ (\frac{g}{mol})}{6}$$

Equation 3: This calculation was used to determine the amount of ligand needed to be used to for a 1:1 exchange in molar concentration. It was then adjusted to give other desired ratios used in this paper.

The amount of dodecylamine solution added was determined by the concentration of the solution (Equation 3). A compensatory amount of toluene was added to the lower concentrations to make all solutions have an equivalent volume.

2.2.4.2 Ligand Exchange Process

For the ligand exchange, as described in Table 1, 3 mL of the purified solution were split into 6 separate 2 mL vials with 500 µL in each. In a separate 20 mL vial, 0.104 g of dodecylamine (DDA) was dissolved in 10 mL of toluene creating a colorless solution. Using the ratios described above the DDA solution was added to each vial and left to sit for 24 hours. It was then purified as described previously and redissolved in 250 µL of toluene.

2.3 Characterization

2.3.1 UV-Vis

For the preparation for spectroscopy, 3 mL of the cadmium selenide solution was taken out of the stock solution and purified as explained previously. The precipitated QDs were then dissolved in 3 mL of toluene and placed in a quartz cuvette. The spectra were taken from 700 nm to 300 nm. As a result of this, the batch concentration was found to be 1.86×10^{-6} M.

$$D = (1.6122 \times 10^{-9})\lambda^4 - (2.6575 \times 10^{-6})\lambda^3 + (1.6242 \times 10^{-3})\lambda^2 - (0.4277)\lambda + (41.57)$$

Equation 4: Where D is the size of the nanocrystal and λ is the wavelength of the first exitonic peak in nm of the CdSe sample.[23]

2.3.2 TEM

For the preparation for TEM, 250 µL of the cadmium selenide solution was taken out of the stock solution and purified in a similar manner as explained previously; this time after adding the equivalent amount of toluene and drops of acetonitrile, it was placed in a 1.5 mL centrifuge tube before precipitation. The CdSe was then dissolved in 1 mL of toluene. At this point, a copper/carbon TEM grid was placed on a piece of filter paper and the QD solution was slowly deposited dropwise onto the grid with a 10 µL pipette and left to dry.

2.3.3 DART-MS

The DART-MS system consisted of a Thermo LTQ XL MS from Thermo Scientific with a DART ion source from IonSense Inc. and an IonRocket temperature gradient system and copper "pots" from Biochromato. The *m*/*z* range was set to collect data from *m/z* 100-1000. In the sample preparation for DART-MS, 5 µL aliquots of the previously purified CdSe solution were pipetted into a copper "pot" which was used as the vessel for the instrument. It was then left to dry under open air for approximately 10 minutes. The DART ion source was set to heat He gas to 400 °C

and the IonRocket temperature program was set to control the sample heater for 0.2 min at 30 ℃ before ramping up to 500 ℃ at a rate of 100 ℃. At 500 ℃ it is held for 0.5 min before the end of the analysis.

Figure 7: This copper pot from Biochomata has a volume of 5 µL.

CHAPTER THREE

3.1 Data

When analyzing thermal desorption DART-MS data there are three main aspects that are important in the identification of molecules: the Total Ion Chronogram (TIC), Extracted Ion Chronogram (EIC), and mass spectra. The TIC shows the combination of the signal of all ions within a sample as a function of time. The EIC shows the signal of a selected range of values surrounding the ion of interest (i.e., a single *m/z* value) versus time. In this thesis, the range of the shown *m/z* is ± 0.5 from the selected *m/z* peak.

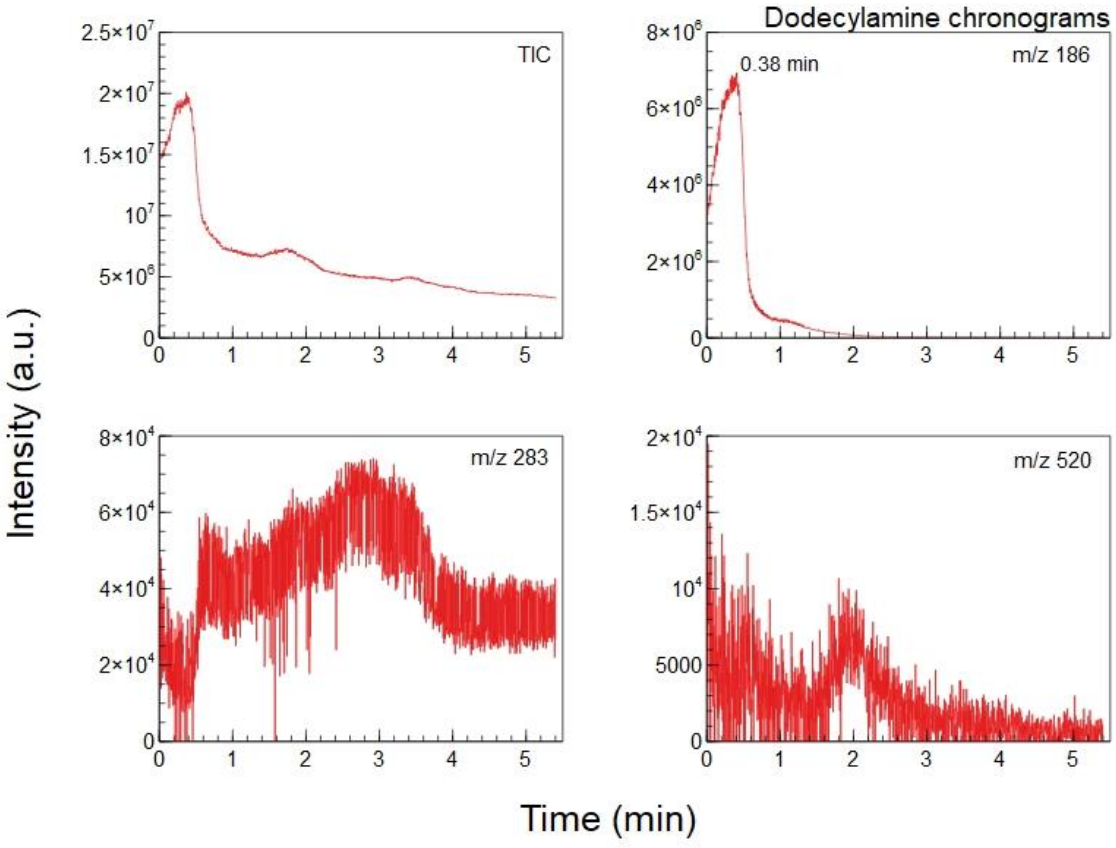

Figure 8: Thermal desorption DART-MS data of dodecylamine (6 mg of DDA in 10 g of toluene) collected in positive mode. Top left: TIC. Top right: EIC at *m/z* 186 Bottom left: EIC at *m/z* 283 Bottom right: EIC at *m/z* 520

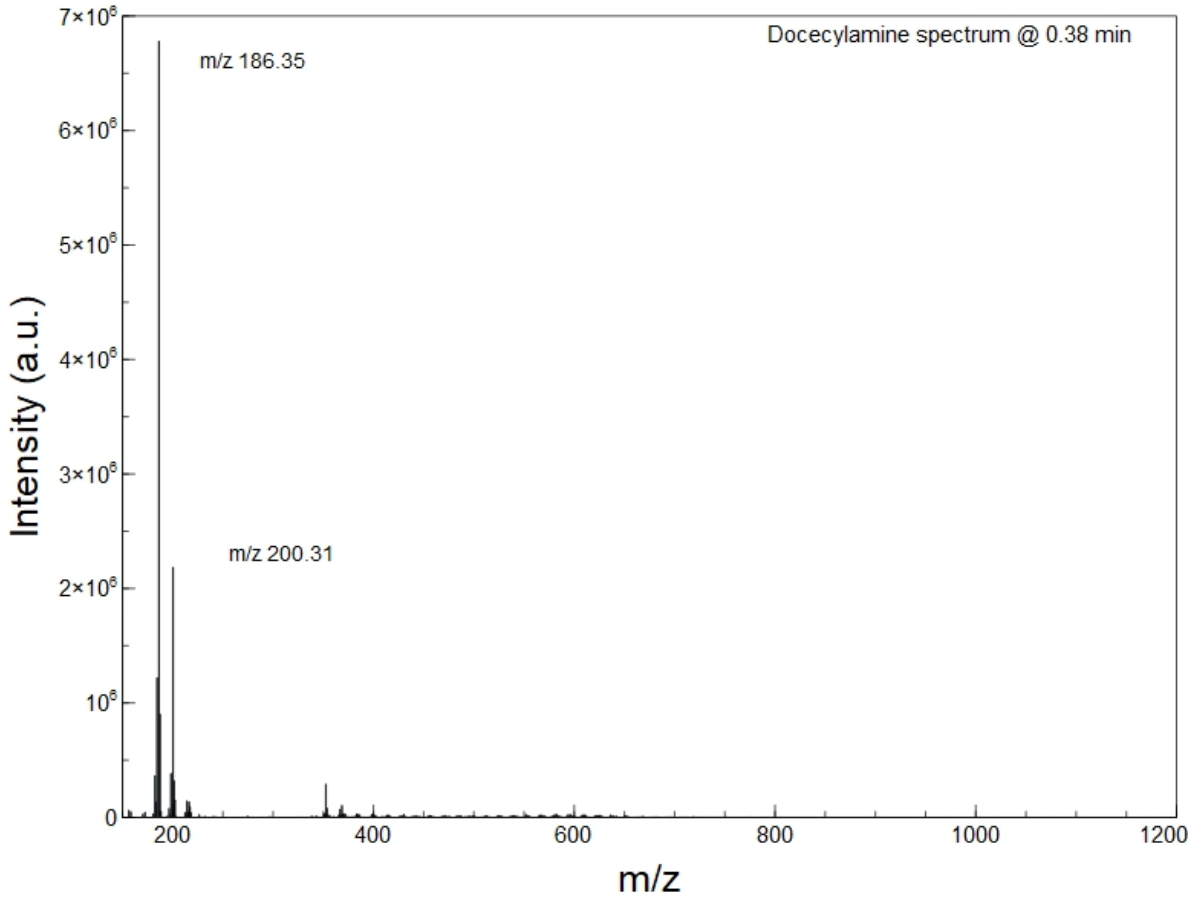

Figure 9: Mass spectrum of dodecylamine collected in positive mode at 0.38 min.

DDA is a long-chained amine ligand with a molecular weight of 185.35 g/mol. In positive mode, the detected ion would be the protonated amine ($M+H^+$) giving an *m/z* of approximately 186. The TIC (Figure 8, top left) has a main peak at 0.4 mins. In the scan shown in the EIC of *m/z* 186 (Figure 8, top right) the DDA gives an appreciable signal even at the starting temperature of 30 °C, though that temperature only coincides with the melting point of the ligand. This signal is likely due to DDA vapor present above the liquid sample through the evaporation and the high sensitivity of the instrument. Most of the dodecylamine has been vaporized by 0.4 minutes, which is around 50 °C. The EICs of *m/z* 283 and 520 (Figure 8, bottom left and right, respectively) refer to peaks corresponding to oleates or oleic acids and are not to be expected to have a high signal above the background in this sample. As seen in Figure 8, there are orders of magnitude less signal seen in the EICs of *m/z* 283 and 520 as compared to the EIC of *m/z* 186.

The main peak that is to be followed from this chronogram is the 186 peak and will be used as the identifier of dodecylamine presence during any exchange. The 186 peak, as seen in Figure 9 is clearly seen with a very strong signal in positive mode. The peak at *m/z* 200 is likely caused by the addition of a methyl group.

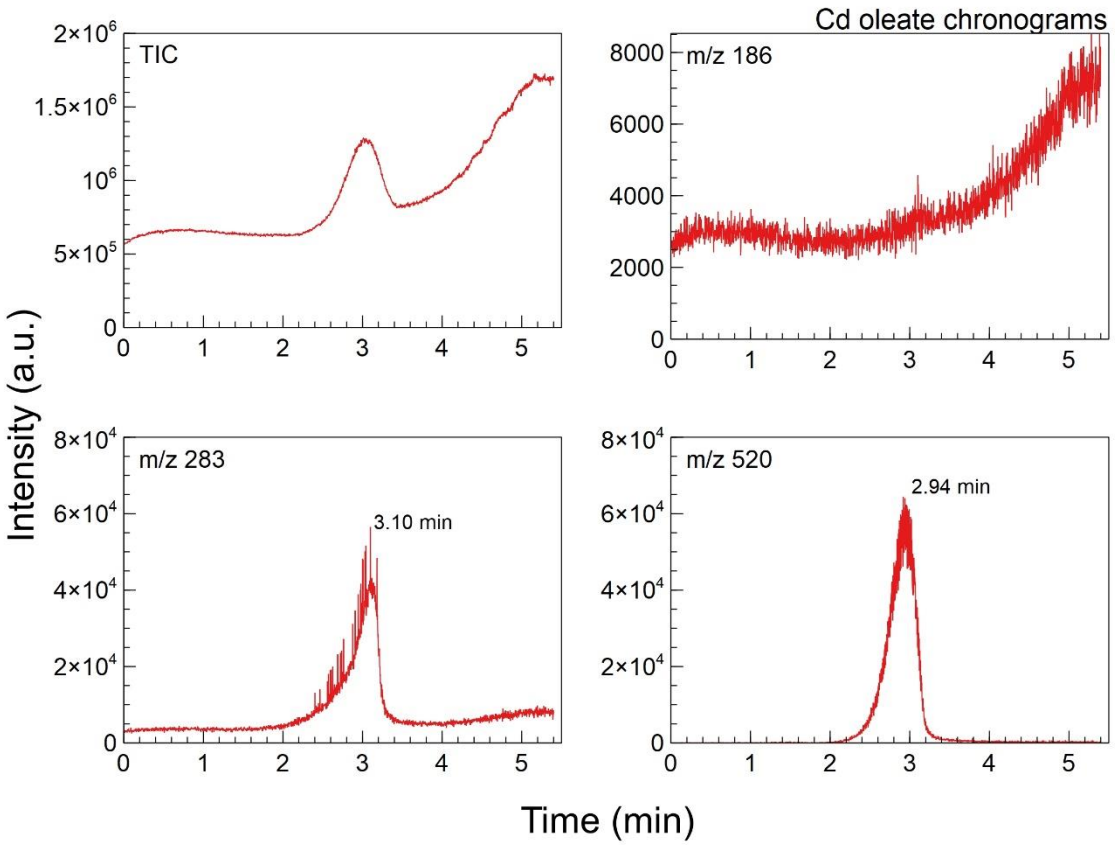

Figure 10: Thermal desorption DART-MS data of Cd oleate collected in positive mode. Top left: TIC. Top right: EIC at *m/z* 186 Bottom left: EIC at *m/z* 283 Bottom right: EIC at *m/z* 520.

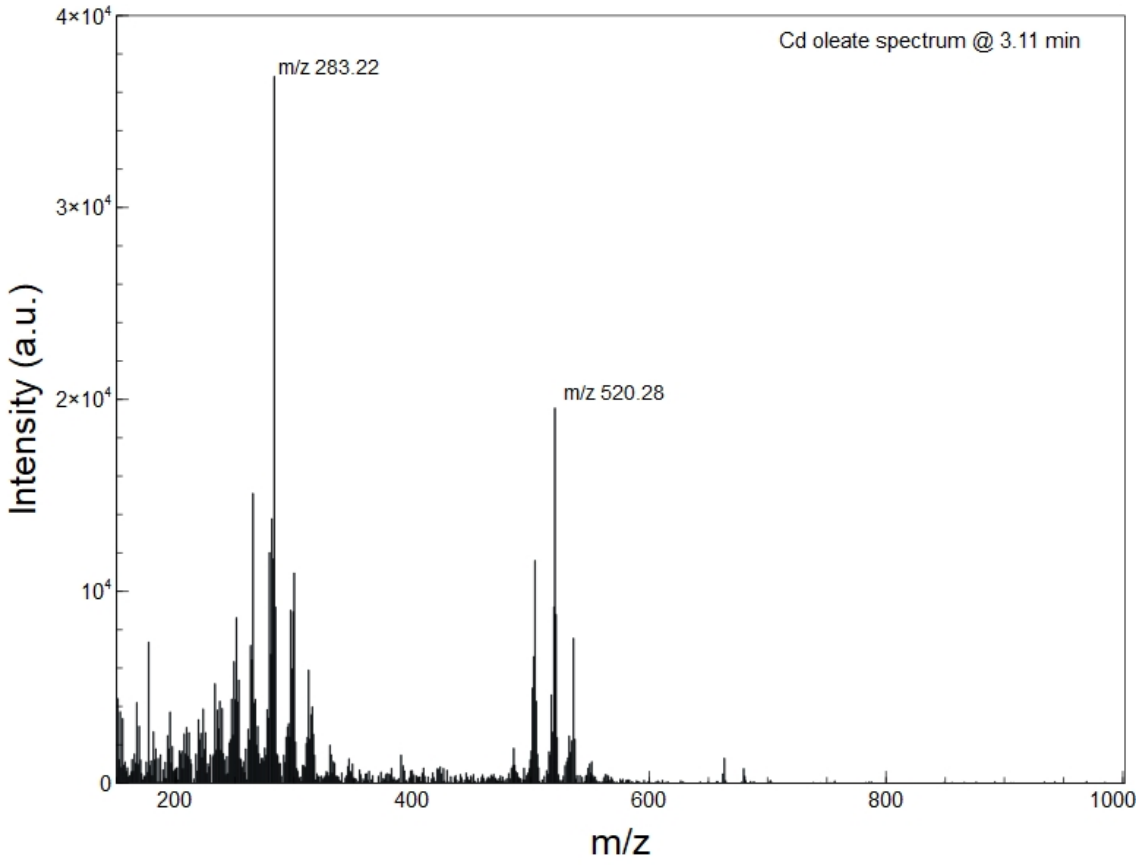

Figure 11: Mass spectrum of cadmium oleate collected in positive mode at 3.11 min.

Figure 10 shows a similar series of data from cadmium oleate. In this figure, a significant peak is seen at 3.1 min in the TIC (Figure 10, top left). When examining the EIC at *m/z* 283 (Figure 10, bottom left) and *m/z* 520 (Figure 10, bottom right) the majority of the signal arises from the two peaks. The EIC at *m/z* 283 peaks at around 3.1 min of the pure, unbound cadmium oleate, corresponding to a temperature of 330 ºC. The EIC at *m/z* 186 (Figure 10, top right) doesn't show any significant peaks and the signal is an order of magnitude lower than the other two EIC selections. As the *m/z* 186 signal in cadmium oleate is sufficiently low as compared to the signal seen in DDA, tracking the change of ligands is easier.

Figure 11 shows the spectrum obtained from the cadmium oleate data at 3.1 min. There are 2 significant peaks seen at *m/z* 283.2 and 520.3. The *m/z* 283.2 peak can be explained by an oleate ion gaining 2 H^+ ions as the *m/z* 281 oleate becomes positively charged after reacting with the ions from the DART ion source. The *m/z* 520.3 peak, which is a peak occurring at a slightly higher temperature (310 °C, 2.9 min) can be explained by reactions with itself and other ions.

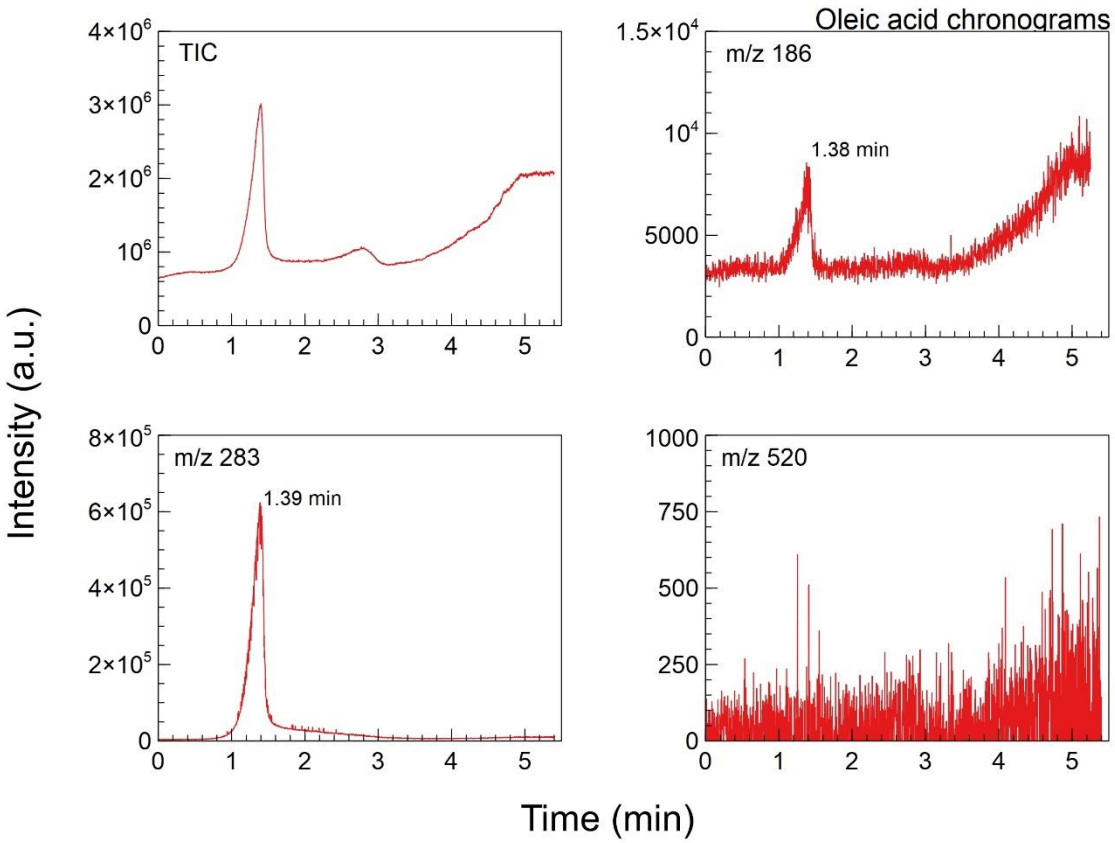

Figure 12: Thermal desorption DART-MS data from 100 ppm oleic acid collected in positive mode. Top left: TIC. Top right: EIC at *m/z* 186 Bottom left: EIC at *m/z* 283 Bottom right: EIC at *m/z* 520.

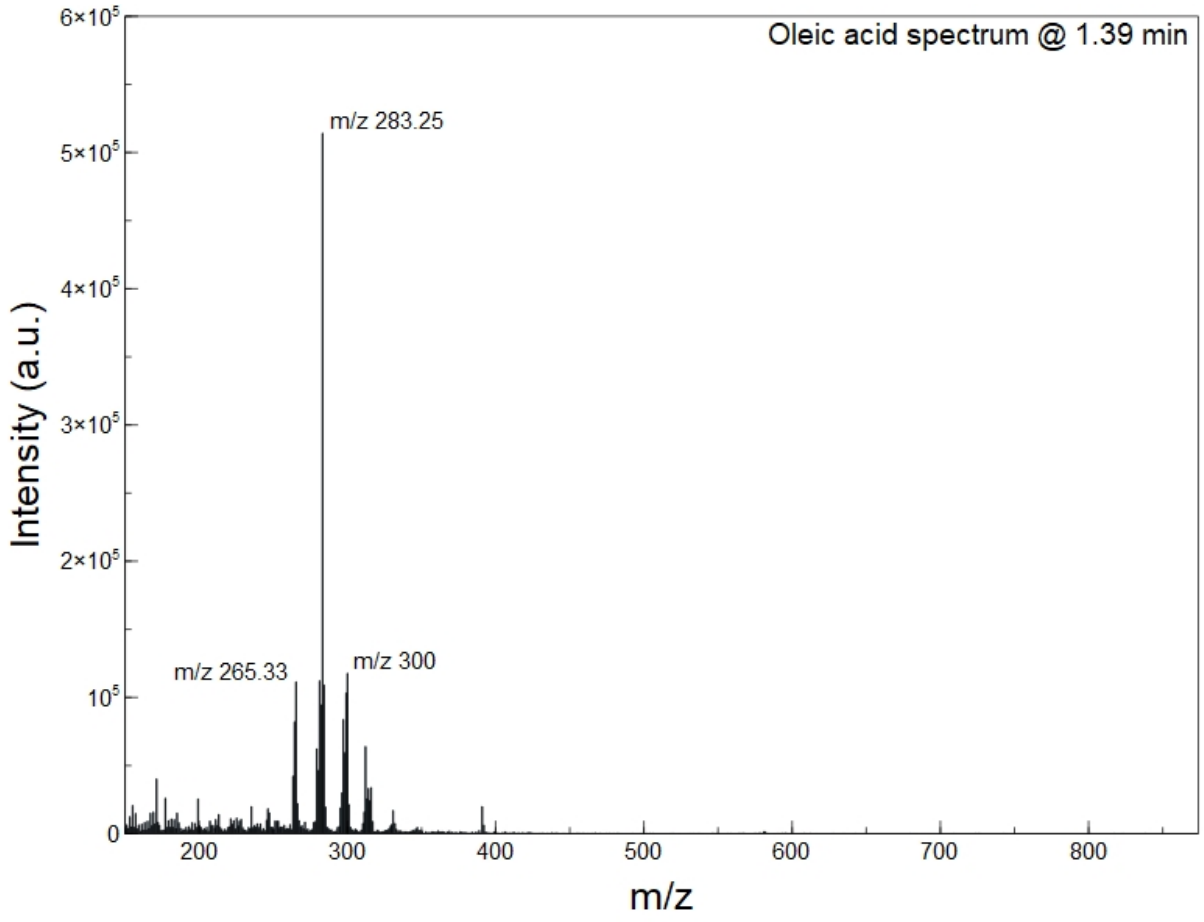

Figure 13: Mass spectra of oleic acid taken in positive mode at 1.39 min.

The EIC at *m/z* 283 for protonated oleic acid (Figure 12, bottom left) showed a significant peak. The EIC at *m/z* 520, however, did not show any signal comparable to what was seen in the cadmium oleate, meaning that *m/z* 520 is a signal unique to the cadmium oleate. As both oleic acid and the oleate have similar peaks at *m/z* 283, a secondary peak that does not interfere with any other signal is needed, which is the purpose the peak at *m/z* 520 serves.

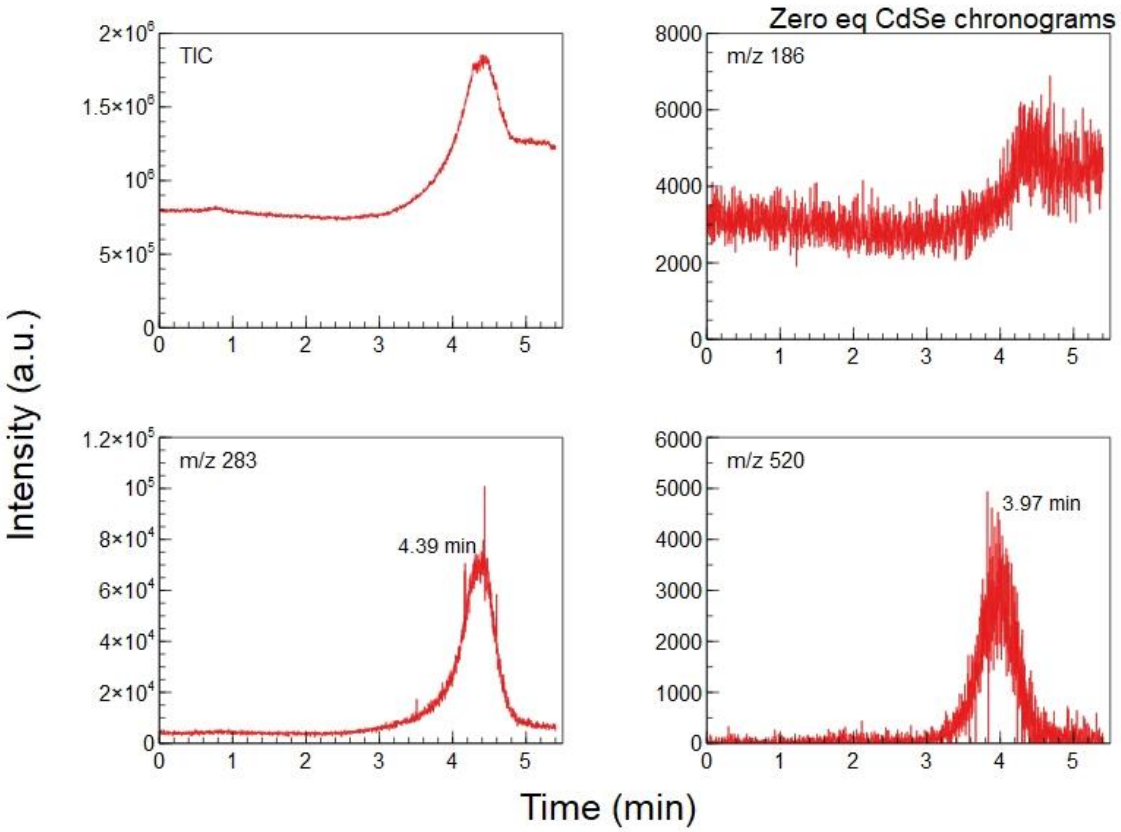

Figure 14: Thermal desorption DART-MS data from oleate-capped CdSe QDs collected in positive mode. Top left: TIC. Top right: EIC at *m/z* 186 Bottom left: EIC at *m/z* 283 Bottom right: EIC at *m/z* 520.

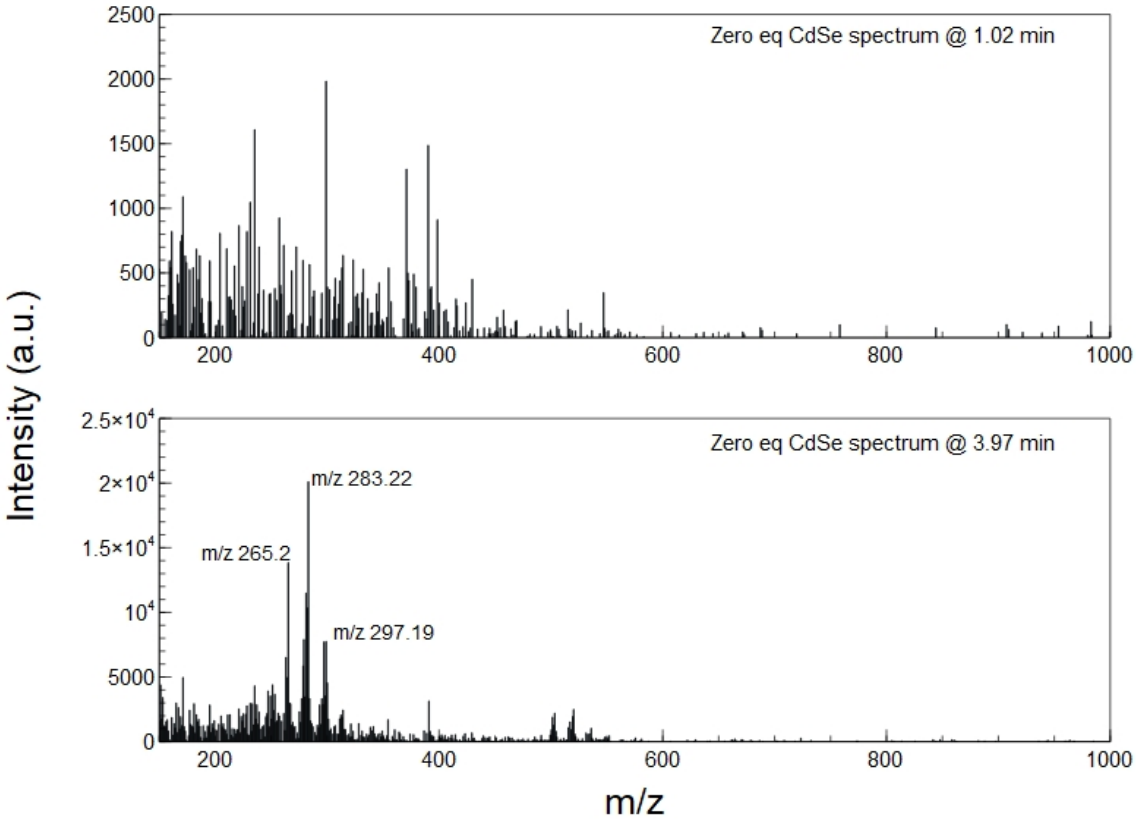

Figure 15: Mass spectra of unexchanged CdSe QDs collected in positive mode at two different times. Top: Mass spectrum at 1.02 min. Bottom: Mass spectrum at 3.97 min.

In the CdSe QDs (Figure 14) it is immediately apparent that no major peaks are visible in the TIC at the beginning of the chronogram. As to be expected, there is no *m/z* 186 peak present in this sample. Additionally, the *m/z* 283 peak now occurs at approximately 4.4 min, which corresponds to a temperature of about 480ºC. This increase in temperature compared to the pure cadmium oleate could possibly be due to the increase in energy needed to remove the oleate bound to the surface of the QD. The *m/z* 520 peak is similarly shifted due to the same phenomena.

In Figure 15, the top figure does not show a signal that rises significantly above the background at 1.02 min, which is where we would find bound DDA. The bottom figure shows a similar mass spectrum as seen in the pure cadmium oleate, however there is a much lower instance of *m/z* 520.

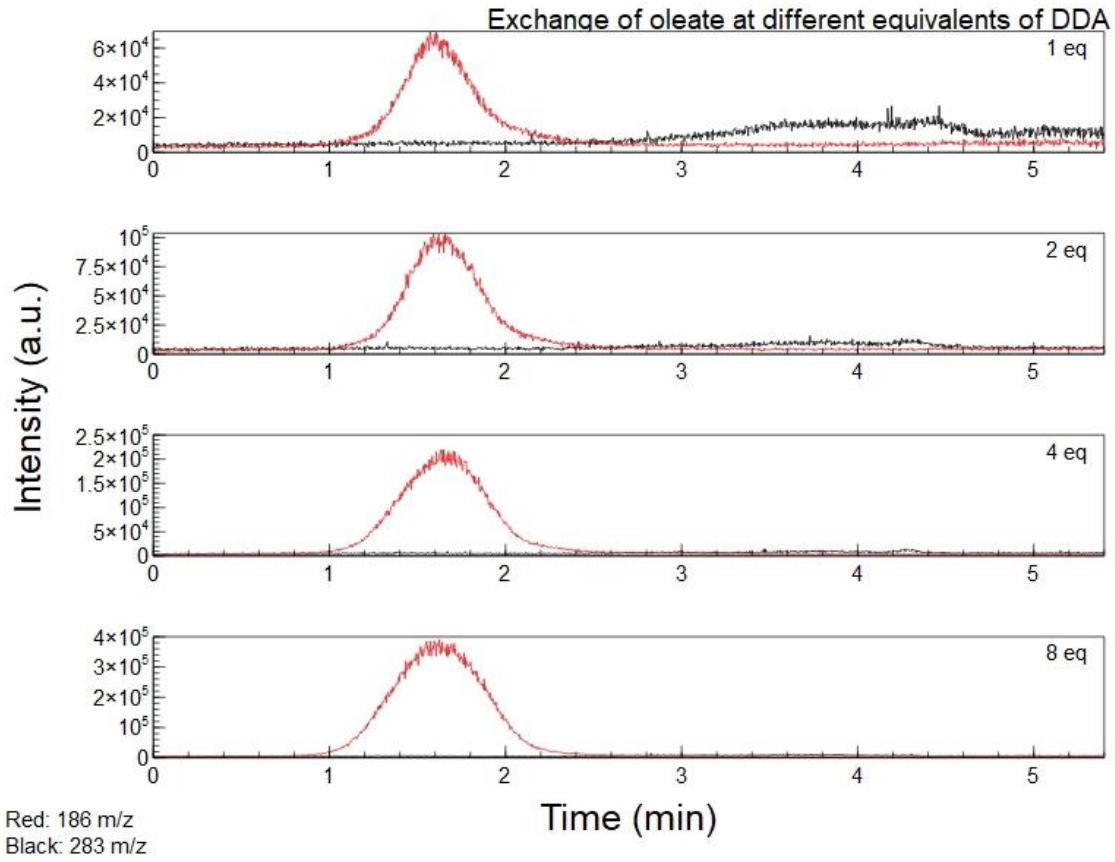

Figure 16: Thermal desorption data of a series of oleate to DDA ligand exchanges from 1 to 8 equivalents for chronograms of *m/z* 186 (red) and 283 (black). Top: 1 equivalent. Second from top: 2 equivalents. Second from bottom: 4 equivalents. Bottom: 8 equivalents.

Figure 16 shows the thermal desorption data from a series of exchanges from 1 equivalent to 8 equivalents of DDA added. The *m/z* 186 and 283 peaks are tracked through the exchange. The max peaks each have slight changes after each exchange, the *m/z* 186 (DDA) increases as you go down the figure and the equivalents of DDA increase. The opposite is true for the *m/z* 283 peak (oleate), the peak decreases as the DDA increases until it is barely noticeable.

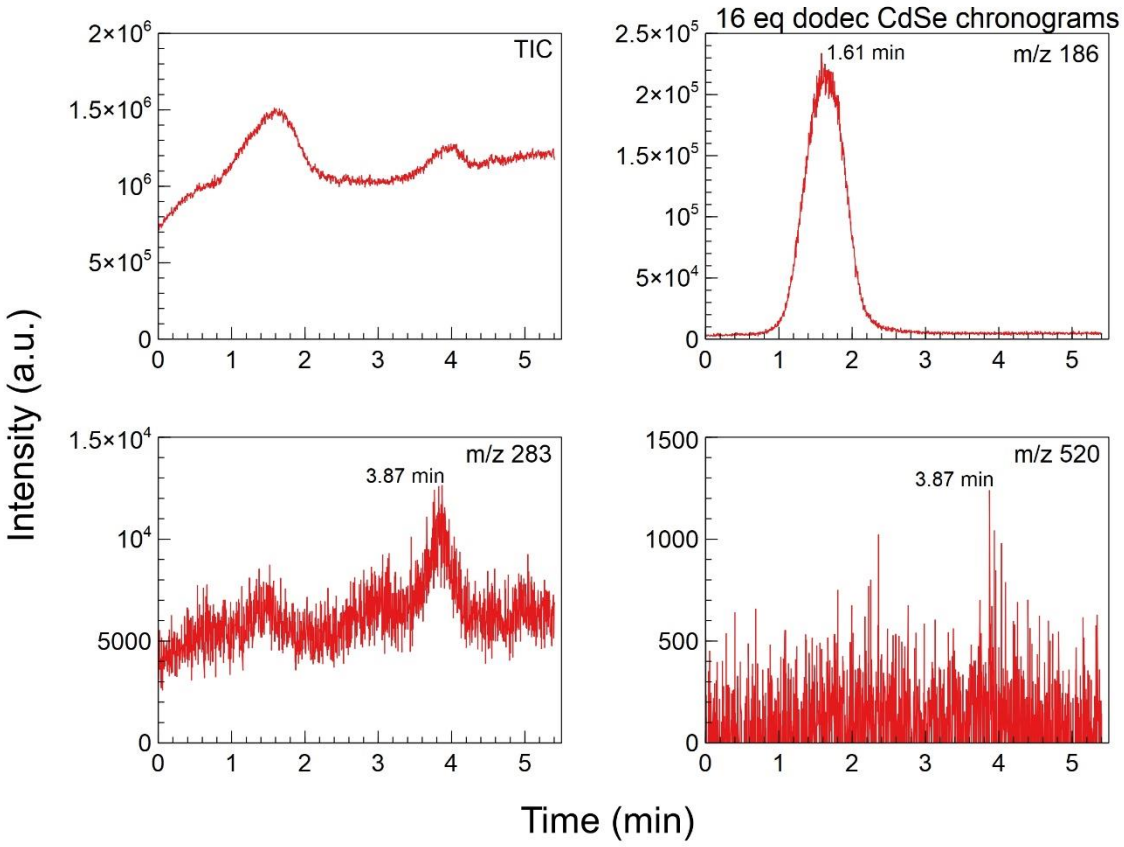

Figure 17: Thermal desorption DART-MS data from CdSe QDs exchanged with 16 equivalents of dodecylamine collected in positive mode. Top left: TIC. Top right: EIC at *m/z* 186 Bottom left: EIC at *m/z* 283 Bottom right: EIC at *m/z* 520.

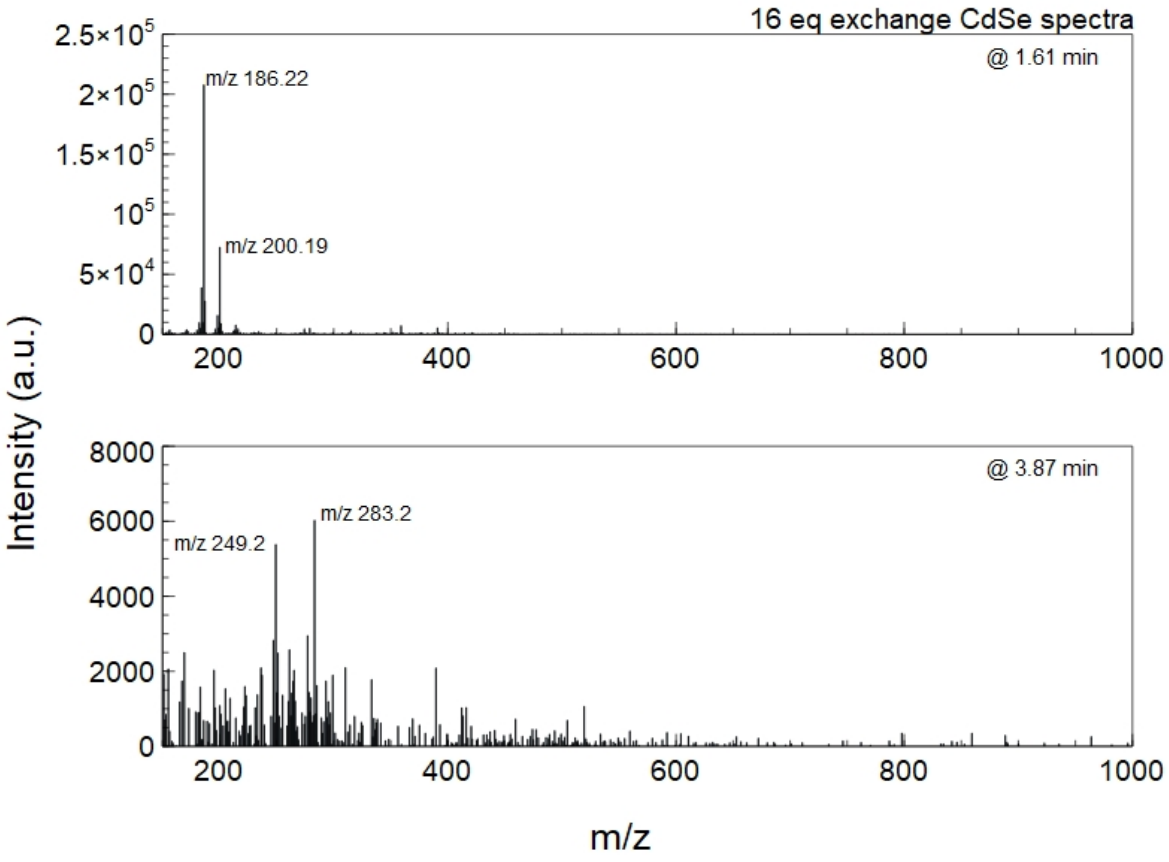

Figure 18: Mass spectra of CdSe QDs exchanged with 16 equivalents of dodecylamine collected in positive mode at two different times. Top: the mass spectra taken at 1.61 min. Bottom: the mass spectra taken at 3.87 min.

Figure 17 shows previously oleate only capped QDs that have had 16 equivalents of DDA added to exchange the ligands on the surface. In the TIC of the 16 equivalents of DDA added QDs, a modest peak is seen at 1.61 min. The *m/z* 186 (Figure 17, top right) EIC shows that the peak corresponds to DDA. This first occurs at nearly one minute or 100 ℃ after the unbound DDA was detected in Figure 8. The bound DDA is detected later than the unbound DDA due to the increased energy needed to remove the ligand from the surface of the QD. The *m/z* 520 and 283 peaks have dropped to a level that is near indistinguishable from the background noise.

Figure 18 shows the mass spectra at 1.61 min (top) and 3.87 min (bottom). At 1.61 min, a peak is clearly seen at the *m/z* 186 corresponding to the DDA peak as shown previously. At 3.87 min, a peak at *m/z* 283 is still seen, however, it is barely higher than a previously unremarkable *m/z* 249 peak, further illustrating the loss of the 283 peak.

3.2 What did not work

3.2.1 Oleylamine

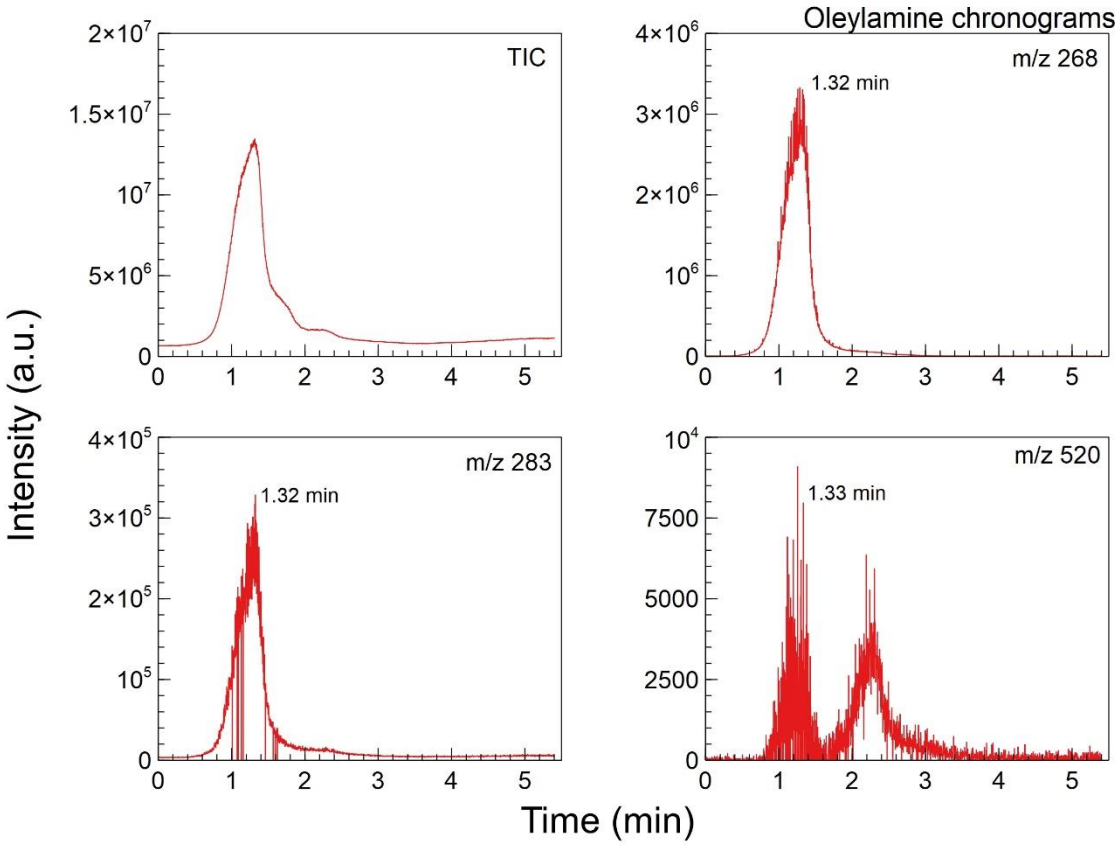

Figure 19: Oleyamine thermal desorption DART-MS data was taken in positive mode. Top left: TIC. Top right: EIC at *m/z* 268 Bottom left: EIC at *m/z* 283 Bottom right: EIC at *m/z* 520.

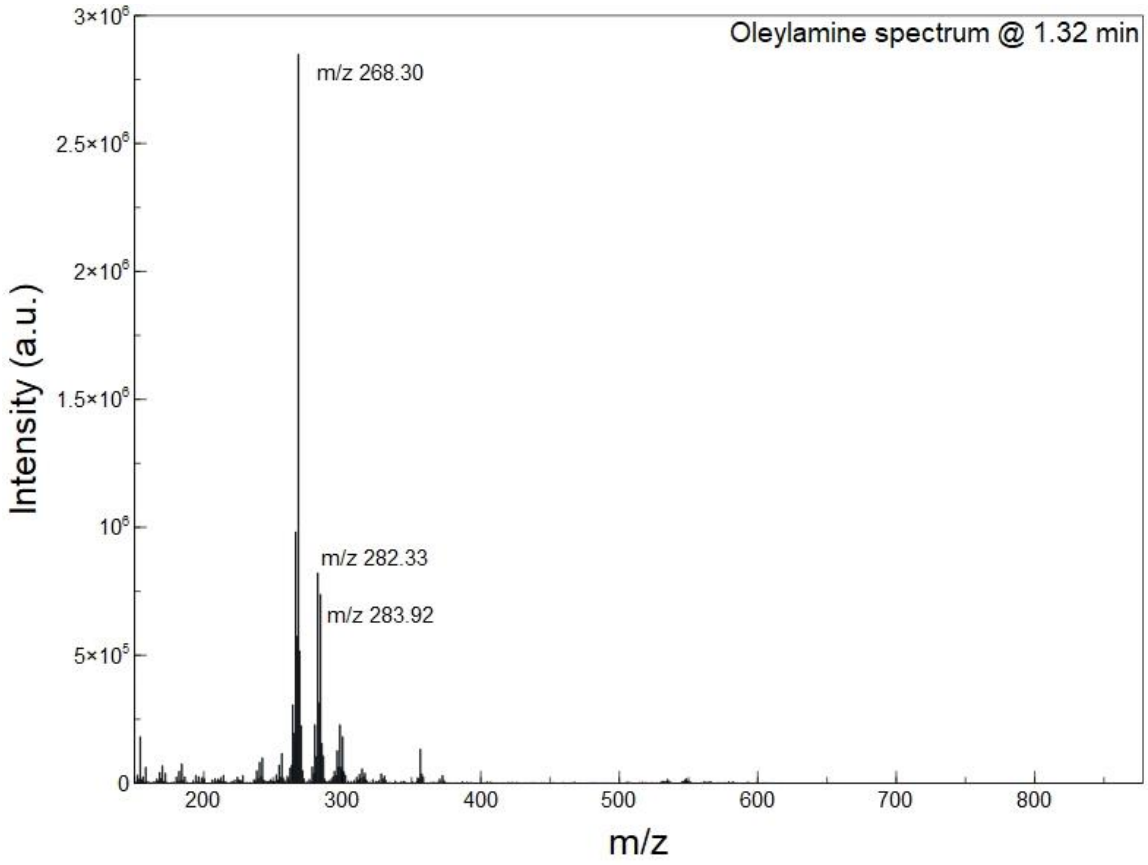

Figure 20: Mass spectrum of oleylamine taken in positive mode at 1.32 min.

Oleylamine was a prospective candidate to be the ligand used to exchange with cadmium oleate in this thesis. There were aspects of oleylamine that were desirable for the purposes of the thesis. The EIC at *m/z* 268 (Figure 19, top right) appears at around 1.32 min unbound to the surface of a QD. This is much earlier than what was seen with the initial cadmium oleate. It is also much less volatile than the DDA, so it comes off the copper pot later and is not immediately detected.

However, during experiments, issues arose that caused it to become a non-viable option. While there is a major peak in oleylamine at *m/z* 268.30 (Figure 20) that does not coincide with the major peaks in the oleate samples, the two secondary peaks at *m/z* 282.33 and 283.92 (Figure 20) would lead to interference at the unit mass resolution of the instrument. The oleate peak as shown in Figure 11 is at *m/z* 283.22, and this would cause an overlap at around *m/z* 283 where distinguishing which signal arises from the oleate versus the oleylamine would be hard to parse out.

3.2.2 Negative mode

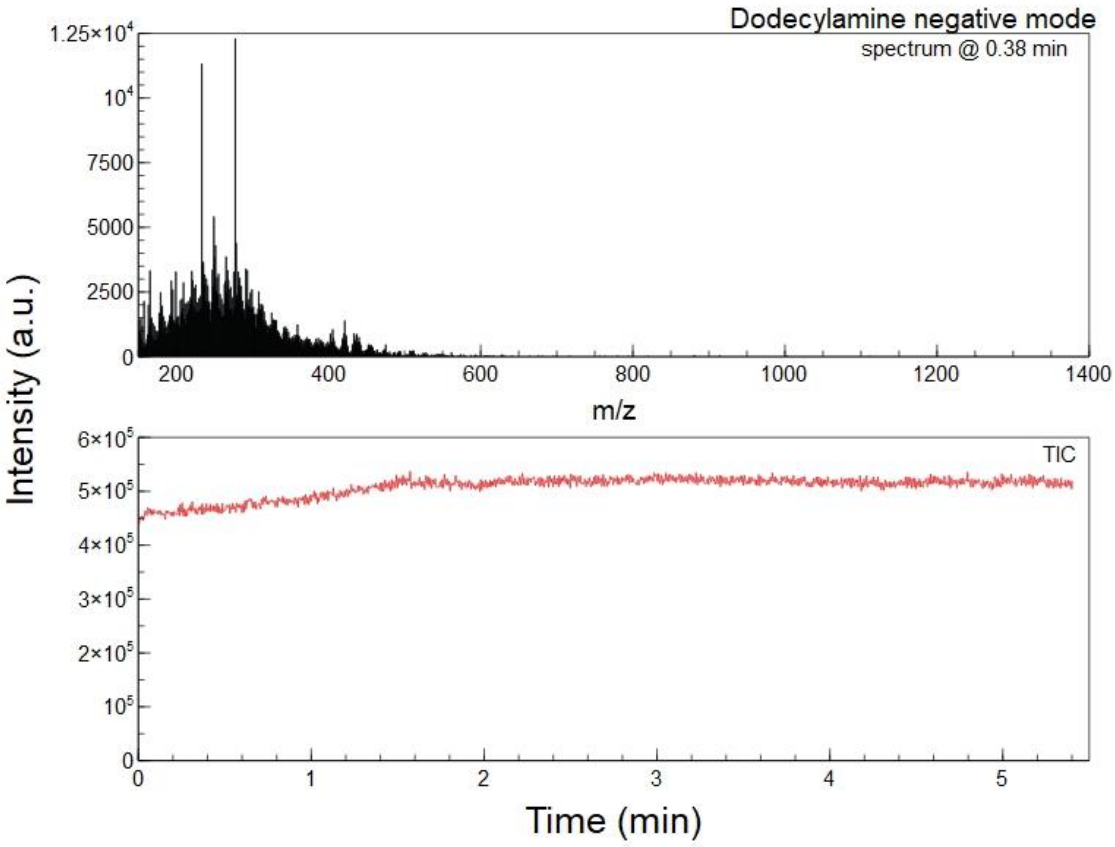

Figure 21: Docecylamine thermal desorption DART-MS data was collected in negative mode. Top: Mass spectrum at 0.38 min. Bottom: TIC

The DART-MS can be operated in both positive and negative modes. However, throughout this thesis, results were only taken in positive mode due to issues arising when detecting in negative mode. The TIC (Figure 21, bottom) of the DDA taken in negative mode is very near a straight line as no signal stands out in the detector. As such, no EIC can be taken out to provide further detail. The mass spectrum (Figure 21, top) shows no significant peak at 0.38 min. The signal is orders of magnitude lower than what was seen in the positive mode samples of DDA. The difficulty of deprotonating the amine group in DDA is likely the cause of the lack of signal.

3.2.3 Quantitative Analysis

The scope of this project included attempts to create a calibration curve that could find the amount of ligand in a solution or on the surface of a QD. This would have also allowed for attempts to track the change of an exchange as a second ligand is added. A lack dueterated solvents needed and less material needed for analysis as compared to other methods were some of the anticipated benefits. Unfortunately, multiple attempts to create a calibration curve ran into issues where acquiring consistent data was unable to be achieved.

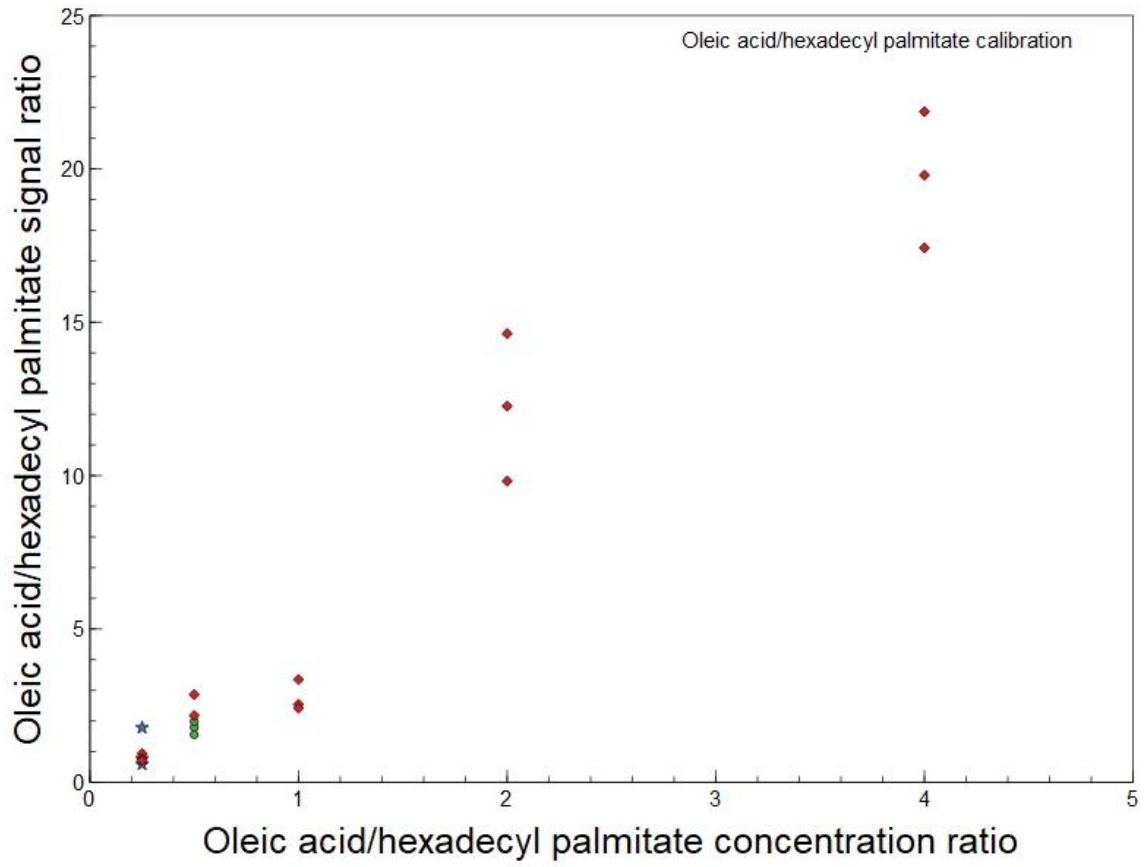

Figure 22: Oleic acid/hexadecyl palmitate calibration

0.25 - a/4b (Blue Star) 2a/8b (red diamond).

0.50 - 2a/4b (green circle), 4a/8b (red diamond).

1 - a/b (red diamond).

2 - 8a/4b (red diamond).

4 - 4a/b (red diamond).

a = 3.125 µg/mL of hexadecyl palmitate, b = mg/mL of oleic acid

This method was done to compare ratios at different concentrations to see that they remained constant between runs. Unfortunately, data was not consistent enough to do further research in this area. Other preliminary attempts at creating a calibration curve with oleic acid were made using octyl octanoate, anthracene, ferrocene, and myristic and lauric acids.

3.2.4 Equilibrium Constant

Finding the binding energy and equilibrium constant also proved to be challenging as we could not get values from the DART that we could be confident enough to compute them. This would only have been possible with the success of the quantitative analysis.

3.3 What it all means

There is a clear addition of DDA onto the surface of the QDs. In Figures 7 and 8, a pure DDA sample is detected by the DART-MS at its peak by 0.38 mins or around 50 ºC. At Figure 14, there is no signal seen at *m/z* 186 on the CdSe before any addition of any DDA. Figure 14 also shows that there is no free DDA in the solution that is detected. In Figure 17, after the addition of DDA to the oleate capped QDs, a signal is seen at *m/z* 186, however, it is at a much later time signature of 1.61 min, which is over 100 ºC higher than the pure DDA. Additionally, an insignificant signal for *m/z* 186 is seen in the 16 equivalents exchanged QDs at 0.38 min as the EIC in Figure 15 shows.

Additionally, loss of oleate is seen, specifically from the surface of the QDs. Figures 9 and 10 show the characteristics of pure cadmium oleate in DART-MS. It has a significant peak of *m/z* 283 that reaches its max at around 3.11 min. Figure 14 shows the unexchanged, cadmium oleate-capped QDs give its max *m/z* 283 signal at 4.39 mins. This is about 75 ºC higher than what is seen in the pure cadmium oleate. In Figure 18, the mass spectrum of the exchanged has a significantly

lower signal of *m/z* 283.2 at 3.87 min as compared to the signal seen at 3.97 min in the unexchanged dots with the *m/z* 283 signal. This loss of signal can be attributed to the loss of cadmium oleate.

Figures 9-14 show the difference between oleic acid, the cadmium oleate in its pure and its bound form. The data shows that oleic acid desorbs at 1.4 min, pure cadmium oleate comes off at 3.1 min, and cadmium oleate on the surface of oleate-capped CdSe comes off at 4.4 min. This occurs due to the increase of energy needed to desorb the long organic chains as the particles become more complex.

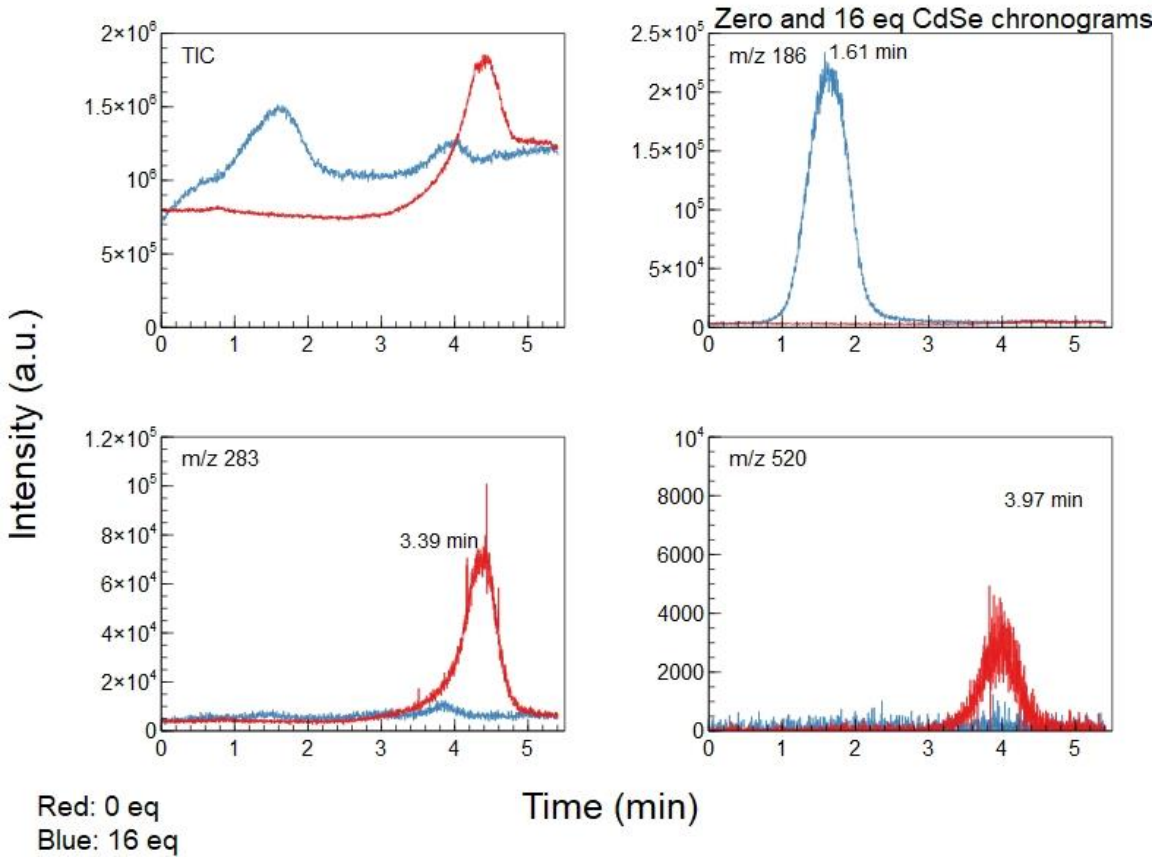

Figure 23: Consolidated thermal desorption data of the zero (red) and 16 equivalent DDA (blue) exchange. In red: zero equivalents. In blue: 16 equivalents. Top left: TIC. Top right: *m/z* 186. Bottom left: *m/z* 283. Bottom right: *m/z* 520.

When taken together, the data show that a change can be seen on the surface of QD during a ligand exchange. Figure 16 shows that the loss of oleate on the surface of QD can be seen as the equivalents of DDA are gradually increased. Figure 23 shows the state of the QD before the exchange and after the addition of the last set of equivalents of DDA at the *m/z* 186 (DDA), 283, and 520 (oleate). The top right of the figure shows that there was no meaningful signal of the DDA peak before the exchange started compared to the 16 equivalents. Also, when comparing the timing that the DDA came off the QDs to pure DDA, there is a significant time jump, meaning that thermal energy is needed to desorb the ligands from the surface. The bottom left of the figure shows the oleate peak dropped significantly by the end of the exchange.

One physical observation that was made is that the solutions with higher concentrations DDA fluoresced less than the solutions of lower concentrations of DDA. This is due to the fluorescence quenching properties of the amine becoming more dominant on the surface of the QDs.

3.3.1 Comparison to NMR

When tracking the exchange of ligands across the surface of QDs, NMR is a common choice. One of the downsides of NMR is that differentiating between similar functional groups can be difficult to determine. This leads to problems when trying to determine the extent of the exchange that has taken place. Additionally, deuterated solvents are needed to complete the analysis, which can be expensive. A large sample is also needed for the analysis to occur. There must also be an extremely high degree of purity throughout the sample.

While running a DART-MS sample is destructive, only 5 µL is needed to run a single analysis. It is also a very quick process to run, with the samples in this thesis only needing about 5.4 mins to complete the analysis.

CHAPTER FOUR

4.1 Conclusions

Ligand exchanges are an important part of making QDs more suitable for use in many fields and tracking the changes is necessary for the process. Previous methods used NMR among other analytical techniques to examine the surface ligands of QDs. In this thesis a new method to track these changes in DART-MS was successfully employed.

Ligand exchange was undertaken with DDA, replacing the oleate that originally capped the QDs. These QDs were purified and analyzed both before and after the exchange process. Three separate peaks were used as markers to track the exchange of the oleate to the DDA. The DART-MS was able to easily differentiate between oleic acid, oleate, and DDA in bound and unbound forms. Between the thermal desorption and mass spectra from the results, two results were observed. First, proof of loss of the oleate and gain of the DDA throughout the process. Second, proof of the near complete binding of a new ligand and the partial minority binding of the original ligand. Methods currently used are unable to give an accurate percentage of ligand coverage; however, multiple distinct ligand systems can still be easily discerned.

4.2 Future Directions

Future directions include creating an internal standard that could be used in quantitative analysis to determine the amount of a particular ligand that exists in a QD sample, both on and off the dot. This could be useful to find out how much is on the surface of two different ligands during a partial exchange. Additionally, this could be used to determine the exact amount of ligand needed for exchange to go to completion without the need for excessive amounts, as this would be important in preventing waste with more specialized ligands that require more work to synthesize.

Recent research in the lab has shown with the acquisition of a higher resolution detector with the DART that a calibration curve can be made using hexadecylamine and oleic acid or oleate, including oleate seen on QDs. When excluding *m/z* data that does not precisely match the values to 3 decimal places seen in the target compounds, there are more consistent results. This detector has shown that with the ability to detect at a more precise detail – two further decimal places – that background compounds in the air interfered with efforts to get consistent data.

REFERENCES

(1) Ngo, C. Y.; Yoon, S. F.; Fan, W.; Chua, S. J. Effects of Size and Shape on Electronic States of Quantum Dots. *Optical and Quantum Electronics 2006 38:12* **2007**, *38* (12), 981–991. https://doi.org/10.1007/S11082-006-9027-7.

(2) Giansante, C. Surface Chemistry Control of Colloidal Quantum Dot Band Gap. *J. Phys. Chem. C* **2018**, *122*, 18. https://doi.org/10.1021/acs.jpcc.8b05124.

(3) Boatman, E. M.; Lisensky, G. C.; Nordell, K. J. A Safer, Easier, Faster Synthesis for CdSe Quantum Dot Nanocrystals. *J Chem Educ* **2005**, *82* (11), 1697–1699. https://doi.org/10.1021/ED082P1697/SUPPL_FILE/JCE2005P1697W.PDF.

(4) Sargent, E. H. Colloidal Quantum Dot Solar Cells. *Nature Photonics 2012 6:3* **2012**, *6* (3), 133–135. https://doi.org/10.1038/nphoton.2012.33.

(5) Qiu, F.; Han, Z.; Peterson, J. J.; Odoi, M. Y.; Sowers, K. L.; Krauss, T. D. Photocatalytic Hydrogen Generation by CdSe/CdS Nanoparticles. *Nano Lett* **2016**, *16* (9), 5347–5352. https://doi.org/10.1021/ACS.NANOLETT.6B01087.

(6) Jin, L.; Huang, Y.; Ma, Z.; Mao, H.; Li, Y.; Yu, H.; Peng, C. Stable Perovskite Solar Cells with Improved Hydrophobicity Based on BHT Additive. *https://doi.org/10.1142/S179329201950022X* **2019**, *14* (2). https://doi.org/10.1142/S179329201950022X.

(7) Xu, G.; Zeng, S.; Zhang, B.; Swihart, M. T.; Yong, K. T.; Prasad, P. N. New Generation Cadmium-Free Quantum Dots for Biophotonics and Nanomedicine. *Chem Rev* **2016**, *116* (19), 12234–12327. https://doi.org/10.1021/ACS.CHEMREV.6B00290.

(8) Wood, V.; Panzer, M. J.; Halpert, J. E.; Caruge, J. M.; Bawendi, M. G.; Bulović, V. Selection of Metal Oxide Charge Transport Layers for Colloidal Quantum Dot LEDs. *ACS Nano* **2009**, *3* (11), 3581–3586. https://doi.org/10.1021/NN901074R.

(9) Pradhan, N.; Reifsnyder, D.; Xie, R.; Aldana, J.; Peng, X. Surface Ligand Dynamics in Growth of Nanocrystals. *J Am Chem Soc* **2007**, *129* (30), 9500–9509. https://doi.org/10.1021/JA0725089/SUPPL_FILE/JA0725089SI20070523_060359.PDF.

(10) Green, M. The Nature of Quantum Dot Capping Ligands. *J Mater Chem* **2010**, *20* (28), 5797. https://doi.org/10.1039/c0jm00007h.

(11) Boles, M. A.; Ling, D.; Hyeon, T.; Talapin, D. V. The Surface Science of Nanocrystals. *Nature Materials 2016 15:2* **2016**, *15* (2), 141–153. https://doi.org/10.1038/nmat4526.

(12) Wu, W.; Shevchenko, E. V. The Surface Science of Nanoparticles for Catalysis: Electronic and Steric Effects of Organic Ligands. *Journal of Nanoparticle Research* **2018**, *20* (9), 255. https://doi.org/10.1007/s11051-018-4319-y.

(13) Hines, D. A.; Kamat, P. v. Quantum Dot Surface Chemistry: Ligand Effects and Electron Transfer Reactions. *Journal of Physical Chemistry C* **2013**, *117* (27), 14418–14426. https://doi.org/10.1021/JP404031S/SUPPL_FILE/JP404031S_SI_001.PDF.

(14) Pavlovich, M. J.; Musselman, B.; Hall, A. B. Direct Analysis in Real Time—Mass Spectrometry (DART-MS) in Forensic and Security Applications. *Mass Spectrom Rev* **2018**, *37* (2), 171–187. https://doi.org/10.1002/MAS.21509.

(15) Liang, J.; Frazier, J.; Benefield, V.; Chong, N. S.; Zhang, M. Forensic Fiber Analysis by Thermal Desorption/Pyrolysis-Direct Analysis in Real Time-Mass Spectrometry. *Anal Chem* **2020**, *92* (2), 1925–1933. https://doi.org/10.1021/ACS.ANALCHEM.9B04167/ASSET/IMAGES/LARGE/AC9B04167_0008.JPEG.

(16) Lobodin, V. V.; Nyadong, L.; Ruddy, B. M.; Curtis, M.; Jones, P. R.; Rodgers, R. P.; Marshall, A. G. DART Fourier Transform Ion Cyclotron Resonance Mass Spectrometry for Analysis of Complex Organic Mixtures. *Int J Mass Spectrom* **2015**, *378*, 186–192. https://doi.org/10.1016/J.IJMS.2014.07.050.

(17) Frazier, J.; Cavey, K.; Coil, S.; Hamo, H.; Zhang, M.; Van Patten, P. G. Rapid and Sensitive Identification and Discrimination of Bound/Unbound Ligands on Colloidal Nanocrystals via Direct Analysis in Real-Time Mass Spectrometry. *Langmuir* **2021**, *37* (50), 14703–14712. https://doi.org/10.1021/ACS.LANGMUIR.1C02548/ASSET/IMAGES/LARGE/LA1C02548_0007.JPEG.

(18) Hens, Z.; C. Martins, J. A Solution NMR Toolbox for Characterizing the Surface Chemistry of Colloidal Nanocrystals. *Chemistry of Materials* **2013**, *25* (8), 1211–1221. https://doi.org/10.1021/cm303361s.

(19) Zeng, B.; Palui, G.; Zhang, C.; Zhan, N.; Wang, W.; Ji, X.; Chen, B.; Mattoussi, H. Characterization of the Ligand Capping of Hydrophobic CdSe-ZnS Quantum Dots Using NMR Spectroscopy. *Chemistry of Materials* **2018**, *30* (1), 225–238. https://doi.org/10.1021/ACS.CHEMMATER.7B04204/ASSET/IMAGES/CM-2017-042049_M004.GIF.

(20) Hamachi, L. S.; Yang, H.; Jen-La Plante, I.; Saenz, N.; Qian, K.; Campos, M. P.; Cleveland, G. T.; Rreza, I.; Oza, A.; Walravens, W.; Chan, E. M.; Hens, Z.; Andrew Crowther, de C.; Owen, J. S. Precursor Reaction Kinetics Control Compositional Grading and Size of CdSe 1Àx S x Nanocrystal Heterostructures †. **2019**. https://doi.org/10.1039/c9sc00989b.

(21) Fritzinger, B.; Capek, R. K.; Lambert, K.; Martins, J. C.; Hens, Z. Utilizing Self-Exchange to Address the Binding of Carboxylic Acid Ligands to CdSe Quantum Dots. *J Am Chem Soc* **2010**, *132* (29), 10195–10201. https://doi.org/10.1021/JA104351Q.

(22) Jasieniak, J.; Bullen, C.; van Embden, J.; Mulvaney, P. Phosphine-Free Synthesis of CdSe Nanocrystals. *J Phys Chem B* **2005**, *109* (44), 20665–20668. https://doi.org/10.1021/jp054289o.

(23) Yu, W. W.; Qu, L.; Guo, W.; Peng, X. Experimental Determination of the Extinction Coefficient of CdTe, CdSe, and CdS Nanocrystals. *Chemistry of Materials* **2003**, *15* (14), 2854–2860. https://doi.org/10.1021/cm034081k.

APPENDIX

SUPPLEMENTARY FIGURES

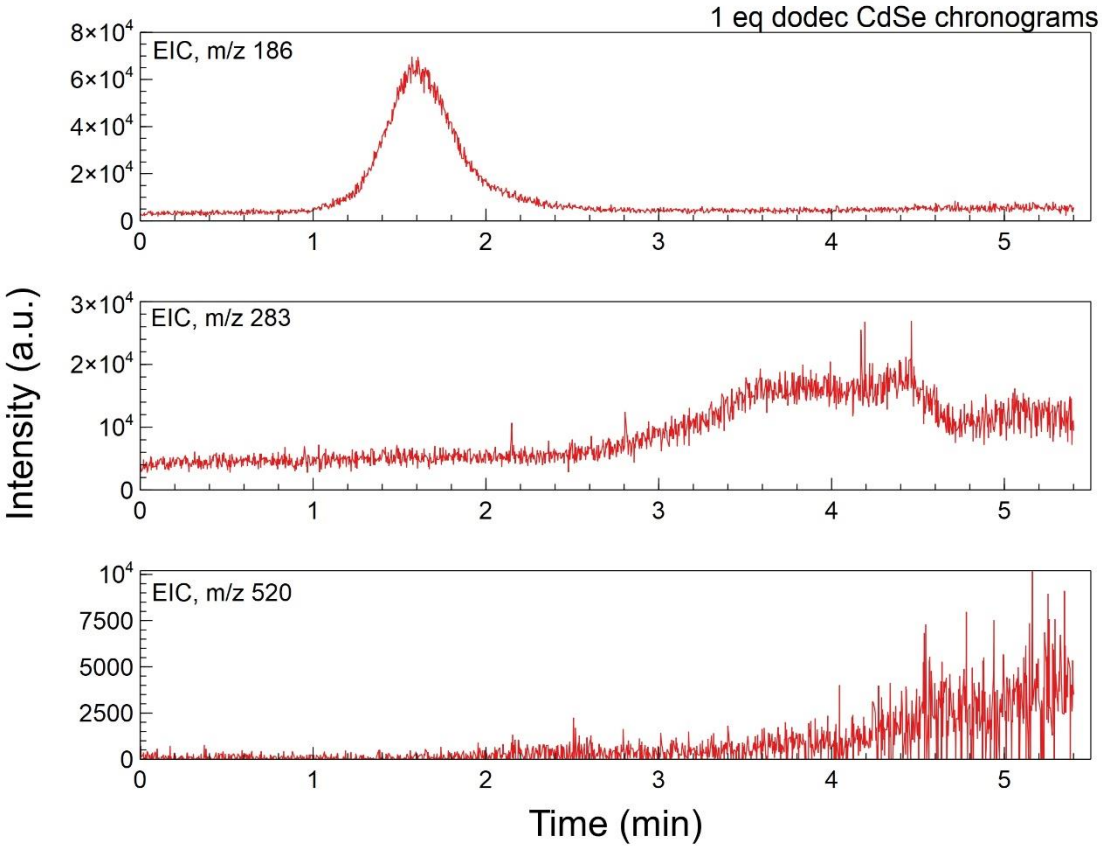

Appendix F1: Figure of the chronograms for the CdSe exchanged with one equivalent of DDA seen at *m/z* 186, 283, and 520.

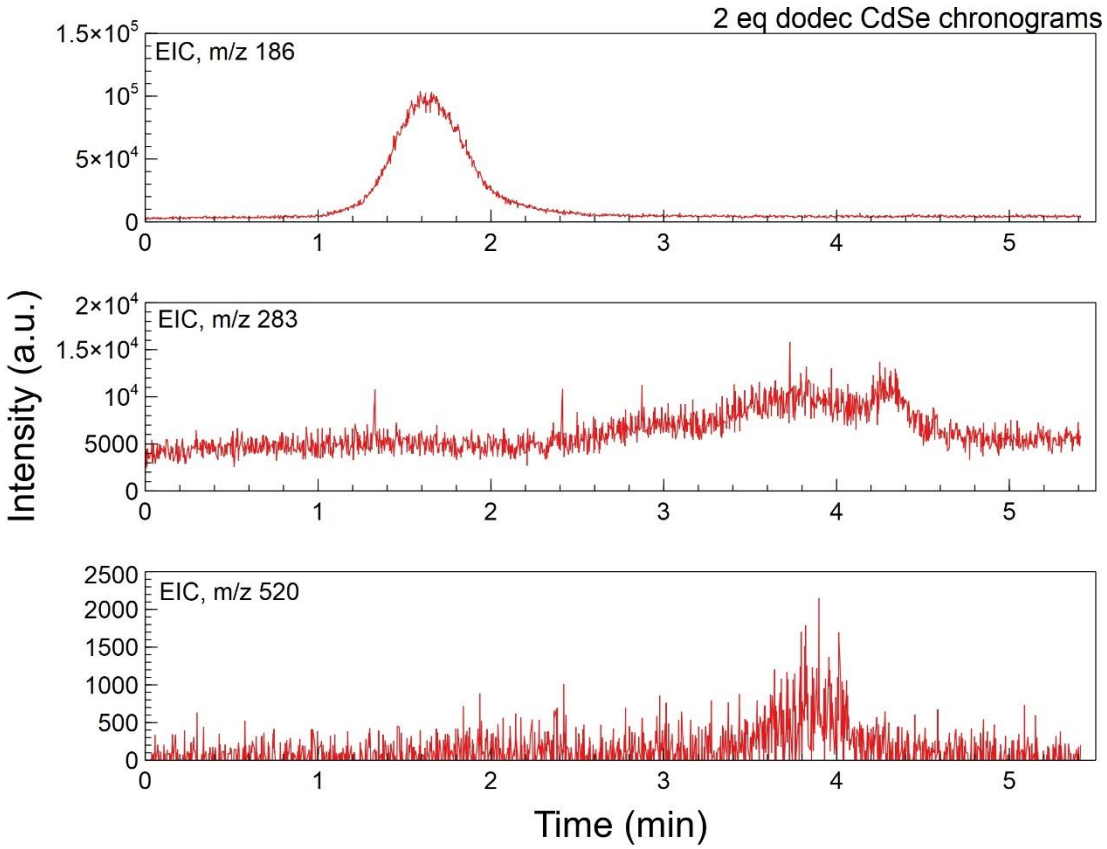

Appendix F2: Figure of the chronograms for the CdSe exchanged with two equivalents of DDA seen at *m/z* 186, 283 and 520.

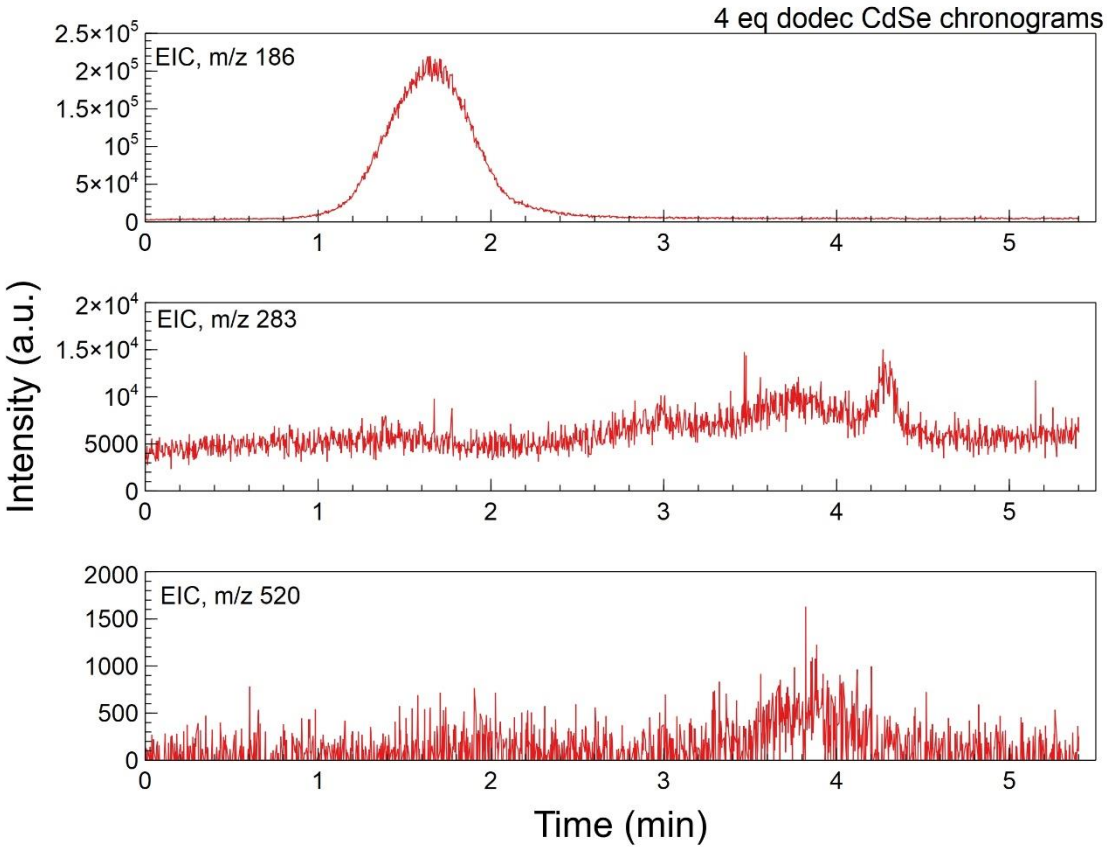

Appendix F3: Figure of the chronograms for the CdSe exchanged with four equivalents of DDA seen at *m/z* 186, 283 and 520.

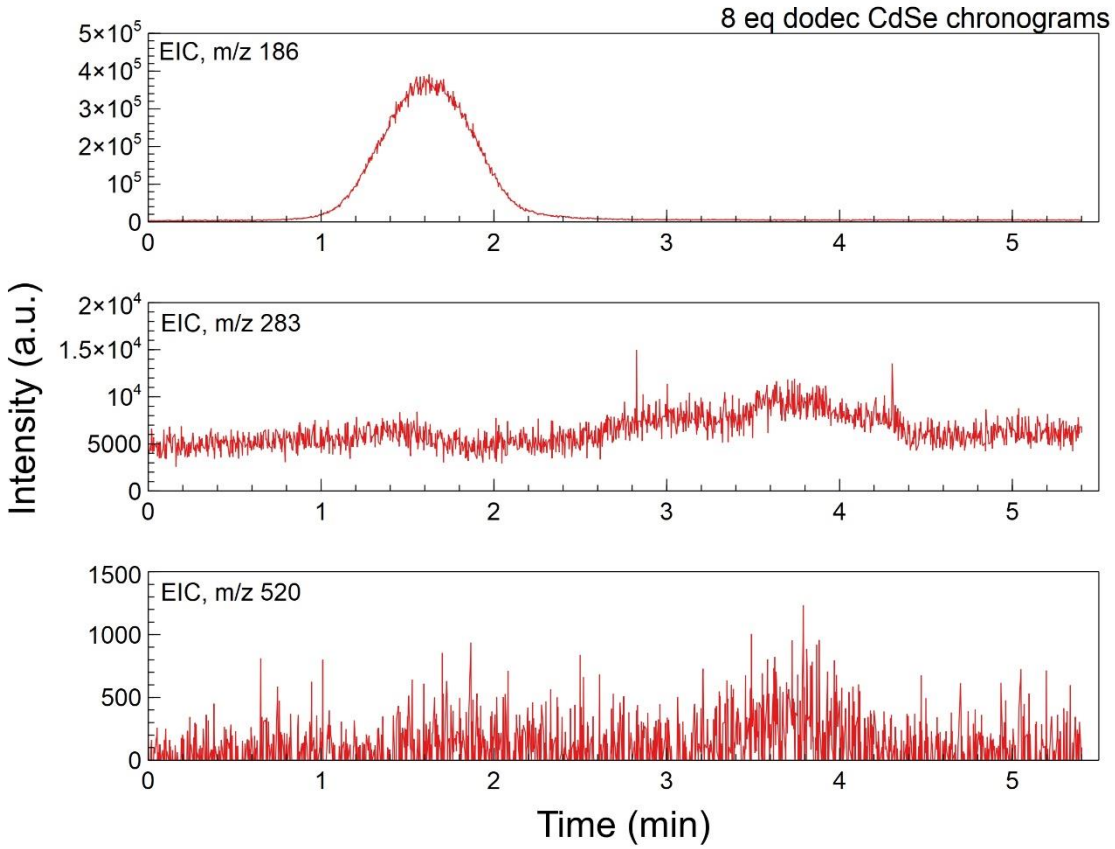

Appendix F4: Figure of the chronograms for the CdSe exchanged with eight equivalents of DDA seen at *m/z* 186, 283 and 520.